Sl. No.	IIT Ropar List of Recent Publications with Abstract Coverage: August, 2026
A	**Book Chapter(s)**
1.	Advances in machine learning for stochastic transport: A perspective of cellular biology and urban transit systems **NK Pande, A Kumar, AK Gupta** - Shaping AI: Ethics, Society, and the Future of Technology: Book Chapter, 2026 **Abstract:** Rapid rise in the technological innovations and a deeper scientific understanding of the complex systems have aided in the development of the field of transportation theory. However, stochasticity is an inherent feature of all transport problems, be it natural or man-made and is difficult to handle theoretically. Machine learning (ML) is one of the major catalysts in reshaping the understanding of the transport phenomena, both from the microscopic cellular level to the urban transit systems. With the influx of data, ML models allow the systems to learn, predict, and adapt to the underlying process, be it the movement of the motor proteins along the cytoskeletal filaments or path planning and routing dynamics of the autonomous vehicles. We describe the integration of the underlying physics of the transport process at both the cellular and macroscale levels with the state-of-the-art deep learning frameworks popularly known as physics-informed deep learning (PIDL). PIDL augments prior physical information of the considered physical system within the deep learning framework, thus generating a robust predictive model. The principal physical laws of the system act as a regularising agent for the model, thus restricting the space of admissible solutions to the desired domain. The experiments performed with the simulated data and the real world have proven the efficacy of the modern deep learning techniques in reliably modelling the transport phenomena. This chapter briefly describes the integration of the PIDL methods with the biological phenomena of ribosome flow and macroscopic modelling of traffic flow.
2.	Assessment of potential glacial lake outburst flood in Uttarakhand using remote sensing and GIS N Sharma, **S Pathak** - Shaping AI: Ethics, Society, and the Future of Technology: Book Chapter, 2026 **Abstract:** Glacial lake outburst floods are a serious hydrometeorological hazard in the rapidly changing Himalayan landscape. This study evaluates the GLOF hazard potential of Kedar Tal, a high-altitude glacier lake in the Gangotri Region of Uttarakhand, India. Multi-temporal satellite imagery (Landsat 5, Sentinel-2) and digital elevation models (SRTM) were utilized to assess lake expansion, terrain attributes, and surface water connectivity to downstream channels. Possible triggering factors were assessed datasets such as USGS seismic records and GPM rainfall were integrated. The lake's area expanded by 53.71% between 1998 and 2025, according to the results and the surrounding slopes are steeper than 35–50, indicating a high risk of avalanches and landslides. Although there has never been a GLOF at Kedar Tal, the environmental factors that have existed over time suggest that there is a moderate to high chance of one. The research suggests the incorporation of Kedar Tal in regional early warning and disaster mitigation plans emphasizes the need of early detection and risk assessment for lesser-studied Himalayan glacial lakes.
3.	Decadal morphodynamic evolution of the Sutlej river basin: A geospatial perspective on channel shifts and basin response S Kaur, **S Pathak** - Geospatial Technology and Advanced Instrumentation in Addressing Water Resources Planning and Management: Book Chapter, 2026

	Abstract: This study investigates the geomorphological dynamics and riverbank instability of the Satluj River along the Jalandhar boundary in Punjab using morphometric analysis and multitemporal satellite imagery from 2014 to 2024. Morphometric parameters derived from SRTM DEM reflect an elongated basin with moderate drainage texture and a low bifurcation ratio, indicating limited structural disturbance but high erosion potential. River channel delineation using Landsat 8 and Sentinel-2A imagery revealed substantial lateral migration, with the left bank undergoing maximum erosion of – 366.47 m (Reach 11) and the right bank showing peak deposition of + 238.77 m (Reach 13). The central reaches (7–13) emerged as critically vulnerable zones, with simultaneous erosion and deposition reflecting unstable channel morphology. These changes are exacerbated by post-2014 flood events and anthropogenic activities such as sand mining and unregulated land use. The findings highlight that the Satluj River is facing accelerated bank erosion, loss of riparian stability, and degradation of adjacent land—necessitating urgent developmental interventions, including sustainable riverbank protection, habitat restoration, and long-term conservation planning.
4.	Implementing LID techniques for runoff reduction through the curve number method considering slope variation in Uttarakhand **S Pathak,** C Bhardwaj - Geospatial Technology and Advanced Instrumentation in Addressing Water Resources Planning and Management: Book Chapter, 2026 **Abstract:** Uttarakhand, a Himalayan state in India, is significantly affected by the flooding in urban regions due to high intensity rainfall, varied land use/ land cover (LULC) and steep topography. This chapter calculates direct runoff estimation by Soil Conservation Service Curve Number (SCS-CN) technique combining LULC, hydrological soil groups (HSG), rainfall and slope data, in ArcMap. Curve Number method formula was used to introduce slope effect on Curve Number (CN) values. In order to reduce runoffs, the Low Impact Development Techniques have been implemented through installing permeable and rain gardens by adjusting CN to capture greater infiltration. The runoff was recalculated after the implementation of LIDs. The results emphasize the effectiveness of integrating slope-based CN modifications and LID practices to reduce surface runoff. This method is used to illustrate the way that sustainable land use planning and hydrological modelling can be combined for better flood risk management in mountainous areas. The methodology offers a replicable model for other regions that are experiencing similar stresses of rapid urbanization and climate change-induced hydrological extremes.
B	**Conference Proceeding(s)**
5.	A user-configurable navigation system for wideness and turn-aware routing **KK Dutta,** VMV Gunturi - 27th IEEE International Conference on Mobile Data Management (MDM), 2026 **Abstract:** Towing increases vehicle length, off-tracking, and turning radius, making narrow streets and right-across-traffic maneuvers particularly hazardous. Recent UK licensing changes allow many drivers to tow without formal training, yet existing navigation systems optimize a single objective such as travel time and largely ignore maneuverability concerns. We demonstrate FlexiRoute, a user-configurable navigation system that enables interactive exploration of safety-time trade-offs under a travel time budget. Given a routing query with a departure-time window, FlexiRoute performs a preference-agnostic, intervalaware search to generate feasible candidate routes and supports instantaneous exploration of alternatives through lightweight reranking rather than re-running search. Time-dependent road width derived from urban clearway schedules, topology-based right-turn semantics, and travel time profiles capture realistic constraints for long or towed vehicles. The demo provides realtime preference switching, Pareto comparison of routes,

	and visual explanations of avoided segments and turns, showing how decoupling search from preference selection enables transparent and usable safety-aware navigation. Demo video link.
6.	Context-aware multimodal depression detection via LLM-derived PHQ-9 personal feature injection H Yang, **P Kumar,** X Li - IEEE International Conference on Image Processing (ICIP), 2026 **Abstract:** Automatic depression detection is important for mental health assessment. Recent multimodal approaches exploit cues from visual, audio and text, but lack explicit injection of clinically meaningful depression context. To address this limitation, we propose a context-aware depression detection method. A depressive personal feature (PF), aligned with nine symptoms from PHQ-9 questionnaire, is fused into a multimodal Transformer. We use GPT to provide soft PF labels, and fine-tune a LLaMA-based predictor with injected domain knowledge to obtain refined PF vectors, which explicitly encode symptom-level depressive context. To enable interpretable symptom-level contributions, dimension-wise gated fusion is employed to inject depressive PF into multimodal representation. Evaluated on the CMDC dataset, the proposed method outperforms baselines with 98.66% F1-score, with loss of interest, appetite change, sleep problem, low energy and suicidal ideation as the most influential PF dimensions, aligning with clinical findings. The results indicate improved performance with context-aware depressive PF injection, while offering better interpretability through symptom-level contributions.
7.	Scalable magnetic tunnel junction arrays for wireless radio frequency sensing and energy harvesting **AS Sandhu, R Sharma, R Sharma** - IEEE International Magnetic Conference-Short Papers (INTERMAG Short Papers), 2026 **Abstract:** Magnetic tunnel junction (MTJ)-based spin rectifiers have emerged as promising low-power solutions for ambient wireless radio frequency (RF) detection and energy harvesting. Traditional series-connected MTJ arrays face scalability challenges due to high effective impedance and distributed interconnect parasitics, leading to impedance mismatch and reduced RF power delivery. Here we present a novel series-parallel MTJ array integrated with a single coplanar waveguide (CPW) acting as an antenna to uniformly deliver RF signals. Using experimentally extracted parasitic parameters, a MTJ array was simulated, demonstrating efficient operation with reflection losses below 50% across
C	**Article(s)**
8.	A DFT study of nitrogen-functionalized double-transition ScMC (M= V/Nb/Ta) MXenes A Pandey, N Sardana - Micro and Nanostructures, 2026 **Abstract:** This work employs first-principles density functional theory for analysing the dynamical and mechanical stability, electronic characteristics using GGA-PBE and HSE06, and energy-dependent optical features for ScMCN 2 (M = V/Nb/Ta) MXenes. ScVCN 2 , ScNbCN 2 , and ScTaCN 2 MXenes are found to be a mechanically and dynamically stable structure. ScTaCN 2 demonstrate the highest Young's Modulus, shear Modulus, and layer Modulus. Both GGA-PBE and HSE06 validate the metallic nature of ScVCN 2 and semiconductor-type characteristics of ScNbCN 2 and ScTaCN 2 MXenes. A higher Poisson's ratio in semiconducting ScNbCN 2 and ScTaCN 2 indicates their potential for flexible electronics. A higher negative value of the real part and a smaller imaginary component in the NIR region in in-plane orientation suggest the suitability of ScVCN 2 MXene for plasmonic applications. The energy gap resulting from the imaginary component of the dielectric function is independent of the in-plane and out-of-plane orientation. ScVCN 2 demonstrates the refractive index below one in the NIR range, showing superluminal propagation.

9.	A strategic approach to drill CFRP composites via configural modifications into the ECDM process N Singh, **T Singh,** SS Sidhu - Materials and Manufacturing Processes, 2026 **Abstract:** This study introduces a strategic methodology for drilling carbon fiber–reinforced polymer (CFRP) composites by modifying the Electrochemical Discharge Machining (ECDM) process. This study assessed the effects of workpiece insulation, tool geometry, and magnetic-field assistance. Insulating the CFRP facilitated localized bubble formation and spark discharges near the tool, thereby reducing the critical voltage and current and enabling through-hole formation with diminished delamination. A diamond-textured tool produced distributed discharges and offered additional abrasive action, leading to a higher material removal rate, reduced hole overcut, and enhanced edge quality compared with a conventional drill-bit tool. The incorporation of magnetic-field-assisted ECDM further improved the electrolyte circulation via magnetohydrodynamic action, disrupted bubble accumulation, stabilized the gas film, and promoted uniform low-intensity discharges. While an increase in voltage enhanced material removal, it also resulted in greater overcut and delamination, particularly in thicker laminates. In summary, the combined application of insulation, diamond texturing, and magnetic assistance markedly enhanced the drilling stability, dimensional accuracy, and hole quality of CFRP composites.
10.	A tutorial on measurement of electrochemical water-splitting performance parameters: Methods and best practices M Sharma, C Prakash, **VK Singh,** A Dixit - ACS Measurement Science Au, 2026 **Abstract:** Electrochemical water splitting has emerged as a promising route to sustainable, green hydrogen production, playing a key role in advancing clean energy systems. The continued advancement of water electrolysis relies heavily on the rational design and evaluation of efficient, durable, and cost-effective electrocatalysts. However, a meaningful and fair comparison of electrocatalyst performance depends on accurate and standardized measurement protocols. This tutorial provides an in-depth overview of the best measurement practices for assessing performance parameters, including overpotential, Tafel slope, charge transfer, electrolyte resistance, electrochemical surface area, turnover frequency, stability, and Faradaic efficiency of electrocatalysts for water splitting. More emphasis is given on highlighting the strengths and limitations of various electrochemical methods, such as linear sweep voltammetry (LSV), cyclic voltammetry (CV), electrochemical impedance spectroscopy (EIS), chronoamperometry (CA), and chronopotentiometry (CP). Further, special attention is given to proper *iR* compensation, selection of appropriate scan rates, and identification of the non-Faradaic region for accurate determination of electrochemical surface area (ECSA). The role of redox peak integration in estimating active site densities, particularly for transition-metal-based electrocatalysts, is also a focus. The transition from standard three-electrode testing to a full-cell alkaline water electrolyzer is also discussed in detail, highlighting standard protocols to minimize the gap between lab-scale testing and commercial-scale electrolyzers. Thus, overall, this tutorial can be considered a practical guide for academicians and researchers, especially beginners in the field, aiming to enhance the reliability of electrochemical measurements and further catalyze the innovation and development of high-performance, energy-efficient water-splitting electrocatalysts for green hydrogen production.

	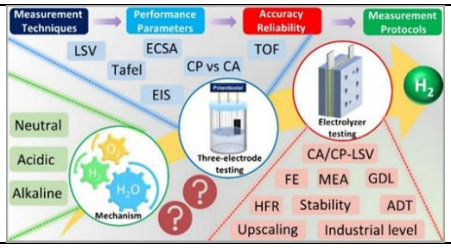
11.	Adaptive behavioural strategies promote species persistence in niche-constrained ecological communities **S Bhandary, PS Dutta** - Proceedings of the Royal Society A: Mathematical, Physical and Engineering Sciences, 2026 **Abstract:** Species persistence in ecosystems results from the interplay between ecological interactions and behavioural strategies. Classical niche theory explains how resource overlap determines the strength of interactions, while evolutionary game theory (EGT) describes how cooperation and defection strategies arise from payoff-dependent decisions. Most eco-evolutionary models assume that strategies remain fixed over generations, overlooking the potential for behavioural adjustments on ecological time scales. Here, we develop a mathematical framework that integrates Lotka–Volterra niche competition (LVNC) dynamics with an adaptive strategy model, allowing species to update their strategies based on the payoff-sensitive Fermi rule. We examine community outcomes on four symmetric games: prisoner's dilemma (PD), snowdrift, stag hunt (SH) and trivial (TR) (also known as harmony), implemented on networks with varying topologies and connectivity. We find that adaptive strategy updates significantly reduce the likelihood of species extinction in comparison to static strategies, enabling coexistence in payoff regions that would otherwise lead to collapse. The structure of the network plays an important role in determining persistence, particularly in snowdrift and PD games. Furthermore, regular ecological networks may experience abrupt extinction with changes in connectivity, whereas scale-free networks support persistence through cooperative hubs. Overall, our results demonstrate that behavioural adaptation is pivotal in promoting species persistence, more so than network architecture alone.
12.	Amorphous erbium oxide (Er_2O_3) memristors with highly linear weight updates for artificial synapses M Malhotra, **MS Yadav, B Rawat,** V Balakrishnan - ACS Applied Electronic Materials, 2026 **Abstract:** An analog memristor with multilevel conductance states is essential for scalable neuromorphic computing, but achieving linear and symmetric SET/RESET switching characteristics for well-defined conductance states remains a major challenge. Here, we report an amorphous erbium oxide (Er_2O_3)-based memristor that addresses this challenge through stable low-voltage bipolar analog resistive switching, highly linear synaptic weight updates, and biologically realistic plasticity emulation. The Au/Er_2O_3/FTO memristor exhibits more gradual resistive switching with ultralow SET and RESET voltages of –0.49 and 0.54 V, respectively, while maintaining low cycle-to-cycle and device-to-device variability, robust endurance exceeding 10^4 switching cycles, and a fast switching speed of approximately 50 ns. Physics-based electrothermal simulations reveal that the analog switching behavior originates from spatially distributed oxygen vacancy migration and the gradual formation and rupture of conductive filaments within the amorphous oxide matrix, which collectively suppress stochastic variability. The memristor further demonstrates excellent synaptic plasticity with low nonlinearity factors of long-term potentiation (NL_P) = 0.74 and long-term depression (NL_D = 0.47), a high symmetricity of approximately 89%, large dynamic conductance windows of 9.2 and 6.5, and an effective conductance-state utilization of nearly 91.4%. In addition, system-level evaluation within the

	artificial neural network and convolutional neural network implementations yields inference accuracies of approximately 95 and 89% for the MNIST and CIFAR-10 datasets, respectively, confirming the suitability of Er_2O_3 memristors as synaptic elements. These results establish amorphous Er_2O_3 as a promising resistive switching material for next-generation analog memory and large-scale neuromorphic computing systems. 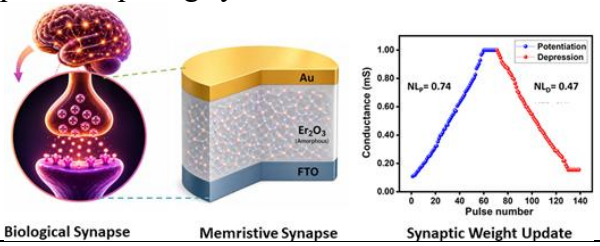
13.	Assessment of multi-ion competition on fluoride release from agricultural soils using fractional factorial design **B Thakur, M Raheena, H Nazir, PP Singh** - Discover Geoscience, 2026 **Abstract:** Fluoride contamination in Punjab, India, is an emerging groundwater quality concern, driven by agricultural soils under intensive cultivation and sustained groundwater abstraction. Despite its significance, the mechanisms controlling depth-dependent F− release from these soils and the role of background ionic chemistry remain poorly understood. This study quantifies F− mobilization using batch experiments with and without representative background ions, providing a mechanistic evaluation of soil–water interactions governing fluoride desorption in agricultural subsurface environments. Results show that F− release is highest in intermediate subsurface layers compared to surface and deeper layers, indicating depth-dependent geochemical controls on mobilization. Variations in soil pH and organic matter content were identified as key drivers governing this vertical heterogeneity. Experiments without background ions exhibited higher F− release rates, highlighting the strong regulatory role of coexisting ions on sorption–desorption dynamics. The effects of six ions (SiO 3 2−, PO 4 3−, HCO 3−, SO 4 2−, Ca 2+, and Cl−) were systematically evaluated in single-and multi-ion systems using a fractional factorial design (FFD). Silicate and calcium emerged as dominant controls, with silicate, phosphate, and bicarbonate enhancing F− release, while calcium consistently suppressed it. Sulfate and chloride exerted minor but contrasting effects between single-and multi-ion conditions. Interaction analysis revealed that the combined effect of silicate and bicarbonate (SiO 3 2−× HCO 3−) was the most influential driver of F− mobilization, particularly under low-calcium conditions. Despite being site-specific, the findings offer transferable insight into fluoride-affected subsurface and agro-environmental systems, providing a framework for understanding persistent groundwater fluoride enrichment.
14.	Asymptotic formulas for the coefficients of an -function associated with Hecke eigenforms on certain polynomials NK Godara, **P Tiwari** - Mathematical Notes, 2026 **Abstract:** In this study, we establish asymptotic formulas for the coefficients of an -function associated with a normalized Hecke eigenform of even integral weight on the full modular group. Specifically, we focus on the average behaviour of these coefficients when evaluated at positive integers represented by certain polynomials in.
15.	Atomically dispersed Fe–Nx sites in a triazine–bis (imino) pyridine covalent organic framework enabling bifunctional nitrate-to-ammonia conversion and oxygen evolution KC Ranjeesh, **C Tayal, J Rawat**…**TC Nagaiah,** D Shetty - Chemistry of Materials, 2026 **Abstract:** Electrochemical nitrate reduction to ammonia (NO_3RR) provides a sustainable strategy for simultaneously removing nitrate pollutants and producing carbon-neutral ammonia; however,

	achieving efficient and selective nitrate conversion under neutral conditions while integrating the anodic oxygen evolution reaction (OER) remains challenging. Herein, we report a coordination-engineered triazine–bis(imino)pyridine covalent organic framework hosting atomically dispersed Fe–N_x active sites (Fe–Tta–Dfp) as an intrinsically bifunctional electrocatalyst for coupled NO_3RR and OER. The crystalline π-conjugated framework combines electron-deficient triazine units that promote nitrate enrichment with bis(imino)pyridine coordination pockets that stabilize isolated Fe centers, enabling precise modulation of the electronic structure and catalytic microenvironment. Comprehensive structural characterization confirms long-range crystallinity, hierarchical porosity, preserved framework integrity, and homogeneous atomic Fe dispersion without metallic or oxide aggregates. Benefiting from the synergistic interaction between triazine-assisted nitrate adsorption and coordination-defined Fe–N_x sites, Fe–Tta–Dfp exhibits outstanding NO_3RR activity in neutral 0.1 M $KHCO_3$ containing 0.1 M KNO_3, achieving a Faradaic efficiency of 94.93% at −0.5 V vs RHE with an NH_3 yield rate of 553.57 μg h^{-1} cm^{-2} at −0.6 V vs RHE, while effectively suppressing nitrite formation and eliminating detectable hydrazine. The catalyst also displays excellent operational stability with negligible Fe leaching and sustained activity during prolonged electrolysis. Moreover, the same Fe–N_x centers efficiently catalyze oxygen evolution, demonstrating genuine bifunctionality within a single COF platform. Comparative studies using structurally related control COFs reveal that the cooperative integration of electron-deficient triazine nodes and bis(imino)pyridine-coordinated Fe sites is essential for maximizing catalytic performance. Density functional theory calculations further show that Fe incorporation optimizes adsorption energetics, enhances orbital coupling, and lowers the rate-determining free-energy barriers for both NO_3RR and OER, in excellent agreement with experimental observations. This work establishes coordination-engineered COFs with atomically dispersed metal sites as a versatile platform for multifunctional electrocatalysis, offering a general strategy for integrated nitrogen valorization and sustainable energy conversion. 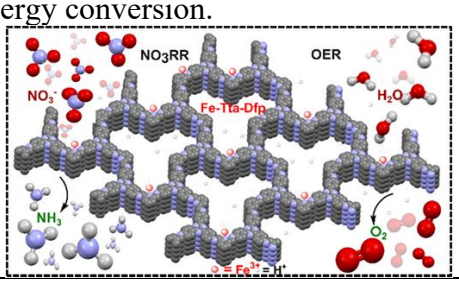
16.	Biaxial strain induced reversible hydrogen storage in 2D boron phosphide biphenylene material **D Dange, P Beniwal, TJD Kumar** - ACS Applied Energy Materials, 2026 **Abstract:** The storage of hydrogen energy is the primary obstacle to its widespread use, underscoring the need for efficient storage materials. Motivated by the increasing prevalence of inorganic biphenylene substitutes, strain-induced modulation of hydrogen storage in 2D boron phosphide biphenylene (BPB) via first-principles calculations is investigated. Pristine BPB is an inefficient substrate for hydrogen storage since the adsorption energy is –0.17 eV/H_2, which falls below the DOE requirement. Thus to further enhance the hydrogen adsorption performance, the effect of the strain on BPB monolayer is studied. Compressive strain enhances bond electronic density, strengthening H_2 adsorption and increasing adsorption energy. On the application of 1.25% biaxial strain, BPB is able to adsorb 24 H_2 molecules, corresponding to 8.8 wt % storage with an adsorption energy of –0.25 eV/H_2. The occupation number analysis provides an understanding of the hydrogen uptake behavior within the strained BPB complex across different temperatures and pressures. The work emphasizes strained BPB as a versatile reversible hydrogen storage 2D material.

	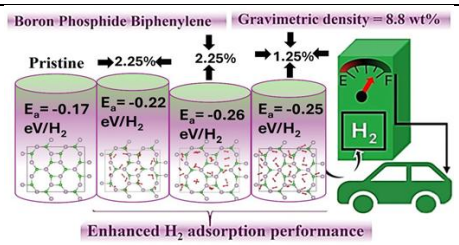
17.	Binder free NiP-textile electrodes for ultrahigh capacity and 40,000 cycle stability in battery supercapacitor hybrid **M Singh, A Kafle, S Mehta, TC Nagaiah** - Advanced Energy Materials, 2026 **Abstract:** Advancement of flexible, high-capacity energy storage systems is vital for next-generation wearable electronics. Cotton cloth with its intrinsic flexibility, porosity, & electrolyte absorption ability, offers an ideal platform, but its insulating nature necessitates functional enhancement. Herein, we report a dual-function, conductive textile electrode (NiP@Ni/NiB-CC) synthesized via electroless followed by electrodeposition eliminating binder serves as both active material & current collector. The designed flexible electrode exhibits an excellent conductivity (1.07×10^4 S m^{-1}) & demonstrated an ultrahigh specific capacitance of 2446 F g^{-1} with 130% capacitance retention over 10,000 cycles at a practical mass loading of 10.1 mg cm^{-2} & delivers an areal capacitance of 45.5 F cm^{-2} at 27.3 mg cm^{-2}. As a current collector for mango-seed-derived activated carbon (MSAC), it enables remarkable stability over 40,000 cycles with 94% retention at 100 mA cm^{-2} and retained 77% capacitance after repetitive mechanical deformations by 1000 bending cycles. The assembled cotton-cloth battery-supercapacitor hybrid (CC-BSH) exhibits an energy density of 441 µWh cm^{-2} & power density of 37.5 mW cm^{-2}. Further two flexible CC-BSH devices successfully powered an LED panel (36 red LEDs) for over 2 h, 50 green LEDs & 50 yellow LEDs showcasing a sustainable, scalable approach for high-performance flexible energy storage.
18.	Catalytic transfer hydrogenolysis of lignin models and native lignin over oxygen vacancy-rich Ni-Ru/HO-TiO_x using isopropanol as a hydrogen donor **A Kumar, R Srivastava** - Energy & Fuels, 2026 **Abstract:** Developing sustainable and hydrogen-efficient catalytic strategies for lignin valorization remains a significant challenge for renewable energy and environmental applications. Herein, we report a defect-engineered, oxygen vacancy–rich Ni–Ru/HO–TiO*x* catalyst for selective catalytic transfer hydrogenolysis (CTH) of β-O-4 lignin model compounds and native hardwood lignin into value-added chemicals and fuels. Surface hydroxyl enrichment and oxygen vacancies are proposed to enhance metal–support interactions, hydrogen spillover, and C–O bond activation over the optimized 3Ni1Ru/HO–TiO*x* catalyst. Using isopropanol as both solvent and hydrogen donor, the catalyst achieved >99% conversion of 2-phenoxy-1-phenylethanol at 160 °C, with tunable selectivity toward aromatic and cyclic hydrocarbons in the absence of externally supplied molecular hydrogen. Mechanistic and kinetic studies suggest that in situ alcohol dehydrogenation, defect-rich interfaces, and modulated surface acidity facilitate hydrogen transfer, selective ether bond cleavage, and controlled hydrogenation. The catalyst showed good stability, recyclability, and minimal metal leaching. Furthermore, the catalytic system upgraded organosolv hardwood lignin into C_6–C_9 cyclic hydrocarbons. CHEM21 green metrics analysis indicated improved material efficiency and reduced environmental impact under optimized conditions. These findings demonstrate the potential of defect-engineered catalysts for sustainable lignin upgrading using catalytic transfer hydrogenolysis pathways.

	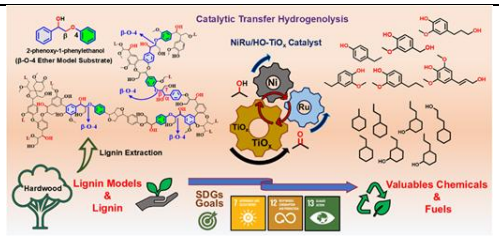
19.	Cavity-interface engineering of spatially programmable exciton–trion populations in monolayer WS_2 B Luhar, Vishal, RK Yadav, **SK, RV Nair**, A Barwal, V Balakrishnan - Materials Horizons, 2026 **Abstract:** Spatially tuned and reconfigurable optical emission in hetero-interfaces of two-dimensional materials remains attractive for opto-electronic and photonic applications. Here, we demonstrate a method to investigate multiple hetero-interfaces in a WS_2 monolayer fabricated in a single sample, spatially engineering the exciton and trion populations. We fabricate WS_2/HfO_2/metal/SiO_2/Si interfaces with metals such as Au, Ni, Mo, and Pt, patterned in a WS_2 monolayer, where the HfO_2/SiO_2/Si stack creates parallel-plate reflectors and traps light, forming a Fabry–Pérot-type cavity. This yields a higher trion-to-exciton ratio of 1.34 in $WS_2/HfO_2/SiO_2$/Si also exhibiting the highest absorption, emission and free carrier density (~3.97 $\times 10^{12}$ cm^{-2}). The WS_2/HfO_2/metal/SiO_2/Si interfaces exhibit optical reflectance and partially trap the light resulting in different population ratios. In contrast, interfaces without the HfO_2 buffer exhibit charge transfer, yielding the lowest trion spectral weight. We demonstrate a unified approach for understanding cavity-interface coupled optical emissions for the fabrication of spatially programmable optoelectronic devices.
20.	Colorimetric nanozyme sensor arrays for food and environmental monitoring: From catalytic engineering to intelligent pattern recognition **M Kumar,** K Sharma, N Kaur, **N Singh** - TrAC Trends in Analytical Chemistry, 2026 **Abstract:** Concerns about environmental contamination and food safety are driving the need for fast, sensitive, and simple screening methods. Conventional analytical methods are highly accurate and reliable, but their routine use is limited due to complex instrumentation, labor-intensive sample preparation, and centralized laboratory facilities. By integrating the multidimensional response capability of array-based sensing systems with the catalytic adaptability of nanozymes, colorimetric nanozyme sensor arrays have emerged as a promising sensing paradigm. Unlike traditional single-analyte sensors, nanozyme sensor arrays rely on interactions between analytes and multiple catalytic components to generate unique colorimetric response patterns. Differences in catalytic activity, substrate affinity, and surface interactions enable these cross-reactive platforms to produce distinct visual fingerprints, allowing differentiation of chemically similar targets. Advances in catalytic engineering—including heteroatom doping, defect engineering, surface functionalization, morphology control, and construction of metal-, carbon-, MOF-, COF-, and hybrid nanozyme architectures—have enhanced catalytic efficiency, selectivity, and signal diversity, improving array performance. The analytical capability of these systems is further strengthened by pattern-recognition methods such as principal component analysis (PCA), linear discriminant analysis (LDA), and artificial neural networks (ANNs). These techniques enable accurate classification and quantitative analysis of toxic analytes by interpreting differences in absorbance spectra, and RGB/HSV features. This paper reviews the design principles, catalytic strategies, and sensing mechanisms of colorimetric nanozyme sensor arrays for detection of food and environmental pollutants. Lastly, prospects for next-generation high-performance nanozyme sensor arrays enabling rapid, reliable, and intelligent food and environmental monitoring are outlined, along with key challenges, emerging opportunities, and future directions.

21.	[Comparative investigations on the role of Hf and Ce on the high temperature oxidation behaviour of β-NiAl alloys at 1200 oC] **S Kumar, PK Ray** - Journal of Alloys and Compounds, 2026 **Abstract:** The effect of Hf and Ce on high temperature oxidation behaviour of β-NiAl alloy is investigated at an oxidation temperature of 1200 o C in presence of ambient air. After 50-hrs of oxidation an exclusive alumina scale develops in both the Hf-doped and Ce-doped alloy. The investigation includes temporal evolution of oxide surface composition, oxidation kinetics, oxide surface morphology and the cross-sectional examinations. Oxidation kinetics result showed that the Hf-doped alloy oxidizes at a slower rate than Ce-doped alloy. Further, the temporal changes in oxide surface composition reveals that, the reactive element such as Hf or Ce present in β-NiAl segregate to the external oxide-gas interface as the oxidation progresses. Results suggest that the ionic transport of Hf cations through the external alumina scale is significantly higher than the Ce cations. The higher transport of Hf cations through the alumina scale further demonstrate that the Hf is more effective in reducing the scale growth behaviour as compared to Ce. The reduction in oxide growth kinetics further leads to the formation of a thinner oxide scale in Hf-doped alloy. In contrast, the relatively low Ce transport to the external surface results in higher growth rate, which facilitates the formation of a potentially thicker oxide scale. 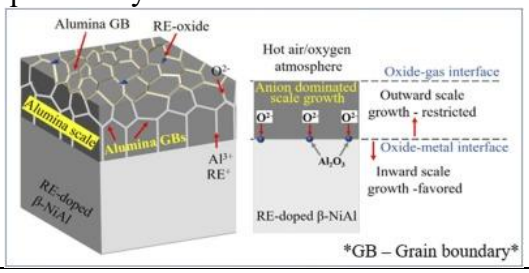
22.	[Defect-engineered Ru/NbCeOx photocatalyst for visible-light-driven lignin valorization to aromatic compounds] **A Kumar, R Srivastava** - Journal of Materials Chemistry A, 2026 **Abstract:** Defect engineering and interfacial electronic modulation offer powerful routes to design visible-light-active photocatalysts for sustainable chemical transformations. Herein, we report a defect-enriched Ru-decorated NbCeOx mixed-oxide Z-scheme photocatalyst in which aliovalent Nb5+ incorporation into CeO2 generates abundant oxygen vacancies and Ce3+ defect states, while highly dispersed Ru nanoparticles promote efficient hydrogen activation and interfacial charge transfer. The synergistic coupling of lattice defects and metal–oxide interfaces significantly enhance visible-light absorption, suppresses charge recombination, and facilitates hydrogen spillover. The optimized Ru(1.5%)/Nb0.2CeOx photocatalyst delivers visible-light-driven hydrogenation and hydrogenolysis performance for lignin-derived model compounds, achieving up to 99% conversion with over 90% selectivity toward partially deoxygenated aromatic products under mild conditions. Spectroscopic and photoelectrochemical analyses, including XPS, UPS, photoluminescence, and scavenger studies, reveal a Z-scheme charge-transfer pathway that preserves strong redox potentials at the heterointerface. The defect-driven strategy is successfully extended to wheat-straw-derived lignin, yielding H-, G-, and S-type aromatic monomers with controlled hydrogenolysis/hydrodeoxygenation. Furthermore, CHEM21 green metrics assessment confirms the favorable environmental sustainability of the developed photocatalytic process under mild visible-light reaction conditions. These findings highlight the catalyst's potential for solar-driven biomass valorization and sustainable chemical production.

	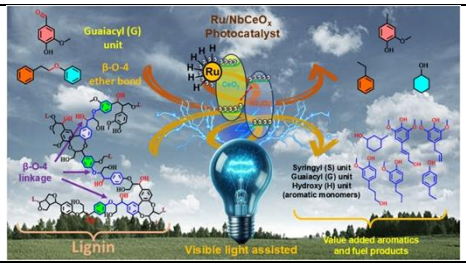
23.	Developing $SrZnO_2$ with *p*-type conductivity by sequential La doping A Sharma, **RV Nair,** AP Singh - Journal of Materials Science: Materials in Electronics, 2026 **Abstract:** Achieving *p*-type conductivity in strontium zincates (SrZnO2) is particularly challenging due to the confined nature of the O 2*p*-derived valence band, which hinders the introduction of shallow acceptors and results in large hole effective masses. In this study, La3+ was selected as a potential dopant to induce *p*-type conductivity. Bulk powder samples of La-doped SrZnO2 (La*x*Sr1−*x*ZnO2, x = 0, 0.03, 0.07) were synthesized and systematically characterized. X-ray diffraction confirmed that the samples predominantly crystallized in the orthorhombic SrZnO2 phase, with a minor SrCO3 secondary phase identified by Rietveld refinement, while Raman spectroscopy provided insights into the vibrational properties. X-ray photoelectron spectroscopy revealed oxygen-related defects and surface chemical states. Hall-effect measurements demonstrated enhanced conductivity with an increase in the La content, supporting the introduction of *p*-type behavior with La doping. Diffuse reflectance spectroscopy showed bandgap energies in the range of 3.22–3.19 eV, confirming visible-range transparency. These findings highlight the potential of La-doped SrZnO2 as a promising *p*-type transparent conducting oxide candidate for optoelectronic applications.
24.	DnCAT: Learning residual denoising and channel attention for accurate RGB-to-HSI reconstruction **S Barda, N Goel -** IEEE Transactions on Computational Imaging, 2026 **Abstract:** Hyperspectral imaging (HSI) has shown great potential in areas ranging from remote sensing to medical imaging due to its ability to capture detailed spectral information across hundreds of bands. However, direct HSI acquisition remains costly and challenging. In contrast, RGB imaging is inexpensive but limited to three bands, restricting its applications. Since both modalities have complementary strengths, reconstructing HSI from RGB offers a cost-effective and practical alternative, making spectral analysis more accessible. Early approaches relied on convolutional neural networks (CNNs), but these often fail to capture long-range dependencies and nonlocal repeating patterns that are essential for accurate reconstruction. Attention-based models have improved results, yet state-of-the-art methods typically suffer from large parameter counts, complex architectures, and limited interpretability. Moreover, attention-based models commonly use multi-scale resolution strategies, which can reduce reconstruction accuracy by losing subtle spatial details. To address these challenges, we propose DnCAT, a transformer in U-shape, designed for HSI reconstruction. DnCAT integrates a transformer encoder-decoder architecture with a bridge module that connects the feature encoder and feature decoder. Its multi-head spectral attention leverages the spatial sparsity and spectral self-similarity of HSI data, improving spectral modeling while significantly reducing parameters. Unlike existing models, DnCAT avoids feature downscaling, preserving fine-grained details crucial for accurate reconstruction. Experiments demonstrate that DnCAT achieves strong performance, with an MRAE of 0.257 and a PSNR of 31.32 representing at least a 2.18% reduction in MRAE compared to previous state of the art methods. These results establish DnCAT as an efficient and reliable benchmark for HSI reconstruction.

25.	Effect of pore structure response on compressibility characteristics of a preloaded soft clayey soil under dry-wet cycles **G Prasad, M Raheena** - International Journal of Geotechnical Engineering, 2026 **Abstract:** The stabilization of soft ground is essential before construction, with preloading being a widely used mechanical method. This study investigates the combined effects of preloading and cyclic drying–wetting (D–W) on the pore structure and compression behaviour of soft clay. Remoulded specimens (0 kPa) and specimens preloaded to 50 and 200 kPa were subjected to one-dimensional consolidation tests. Pore structure evolution was examined using Scanning Electron Microscopy (SEM) and Mercury Intrusion Porosimetry (MIP). SEM revealed a transition from a flocculated, well-packed structure after the first D–W cycle to an open, porous fabric by the sixth cycle. MIP showed a shift from a weak bimodal to a unimodal pore-size distribution. After the first cycle, compressibility decreased by 4.2%, 20%, and 30% for 0, 50, and 200 kPa preloading, respectively, but increased substantially by the final cycle. The results indicate that repeated D–W cycles progressively diminish the benefits of preloading, highlighting its temporary effectiveness in soft-ground stabilization.
26.	Emerging two-dimensional vdW materials and their heterostructures for memristive devices: Advances, challenges, and perspectives **Shiksha, M Kumar** - Advanced Materials Technologies, 2026 **Abstract:** The continuous scaling of conventional CMOS technology has posed critical challenges for modern electronic systems, including high power consumption and limited memory density. The major challenge in current computing systems is the von Neumann bottleneck, which arises from frequent data transfers between memory and computing units, resulting in increased power consumption. These issues emphasize the importance of memristors as next-generation electronic devices capable of meeting the growing demand for energy-efficient and high-performance computation. Memristors provide a solution by combining memory and calculation within a single device, offering nonvolatile data storage and resistance modulation. Researchers explored next-generation 2D vdW materials and their heterostructures as resistive materials for memristors. Here, we present the current advances in memristors based on 2D vdW materials and their heterostructures. Also, analysing their critical resistive-switching behavior under external bias and their suitability for various applications. This review highlights key performance metrics, including power consumption, endurance, retention time, On/Off ratio, and their dependence on material properties and device architecture. Finally, conclude with challenges that limit reliability, scalability, and long-term stability, thereby hindering practical implementation. Furthermore, the existing gaps in memristor research are highlighted, and possible strategies and solutions are proposed to enable the device's realization for future prospects.
27.	Energy-efficient spin hall nano-oscillators using near-compensated CoGd ferrimagnets J Lei, **R Sharma**…H Yang - Advanced Materials, 2026 **Abstract:** Conventional spin Hall nano-oscillators (SHNOs) based on ferromagnets face practical limitations due to high threshold current densities and large external magnetic field requirements. Ferrimagnets provide an attractive alternative due to their unique magnetic dynamics and potential for energy-efficient spintronic devices. In this study, we report rare-earth-transition-metal (RE-TM) ferrimagnetic SHNOs utilizing $Co_{1-x}Gd_x$ alloys, in which compositional tuning enables high-performance operation near the magnetization compensation. The optimized SHNO operates at a low current density (1.43×10^7 A/cm^2), a small magnetic field (5 mT), and exhibits a narrow linewidth (0.61 MHz) simultaneously, showing an order-of-magnitude improvement over its ferromagnetic counterparts. This enhanced performance arises from high spin-orbit torque efficiency, low magnetic anisotropy, reduced effective magnetization, and minimized nonlinearity

	near the compensation point. These results establish RE-TM ferrimagnets as a promising material platform for next-generation spintronic devices and offer new strategies for realizing energy-efficient, high-performance spintronic oscillators.
28.	Enhanced abrupt autofocusing and depth-of-focus of circular airy derivative beams via controlled asymmetry **A Kumari, V Pal** - Optics Letters, 2026 **Abstract:** We demonstrate enhanced abrupt autofocusing and depth-of-focus (DOF) in circular Airy derivative beams through controlled asymmetry. The controlled asymmetry enables multiple discrete autofocusing events to merge into a single continuous elongated focal region with improved energy confinement, thereby enhancing both the abrupt autofocusing and the DOF. The DOF is extended by up to 400 with a 32 improvement in abrupt autofocusing and a 32 μm focal spot size, whereas the abrupt autofocusing can be further enhanced by up to 193 with a 56 μm focal spot size while maintaining nearly the same DOF. This reveals a trade-off between the DOF and abrupt autofocusing ability. Experimental results show good agreement with numerical simulations. The resulting asymmetric circular Airy derivative beams, combining strong abrupt autofocusing with extreme DOF, offer promising applications in optical trapping, optical communications, microfabrication, and biomedical imaging.
29.	Evaluation of liquefaction response of waste foundry sand using energy dissipation approach **A Kumar, S Sharma, N James, A Parihar** - Géotechnique Letters, 2026 **Abstract:** The reuse of waste foundry sand (WFS) as a sustainable alternative to natural sand in geotechnical backfill applications necessitates a thorough understanding of its behaviour under dynamic loading. This study presents an experimental evaluation of the dynamic and liquefaction behaviour of WFS using cyclic triaxial testing. A comprehensive test programme was conducted on cylindrical specimens of 50 mm dia. and 100 mm height under stress-controlled cyclic loading. Tests were performed over a range of loading frequencies (0·1–5 Hz) and cyclic stress ratios (CSR = 0·15–0·25) to simulate seismic and traffic-induced loading conditions. For comparison, selected tests were also carried out on natural silica sand under identical conditions. The response of WFS was assessed in terms of excess pore water pressure generation, cyclic deformation characteristics and the number of cycles to liquefaction. The results indicate a clear influence of loading frequency and CSR on the liquefaction resistance of WFS. Compared with silica sand, WFS exhibits comparable dynamic performance. This study can also be useful for assessing seismic response and stability analysis of WFS landfills.
30.	Experimental analysis on effect of type-2 diabetic mellitus on strength behaviour of trabecular bone structures SS Barekar, TA Jadhav, **N Kumar** - International Journal of Biomedical Engineering and Technology, 2026 **Abstract:** The type-2 diabetes affected bones are more susceptible to fragile fractures due to the deterioration in bone mineral density (BMD). This study aims to investigate the structural integrity of human trabecular bone by comparing nanoindentation-based mechanical evaluation outcomes of three diabetic and two non-diabetic bone samples. The obtained results stated that a 45-year-old T2DM sample has lower modulus of elasticity (40.81%), toughness (34.24%) and diminished bone quality when compared to normal bones. Mechanical analysis shows that T2DM causes mean reductions of the elastic modulus by 5.3 GPa, stiffness to 4.9 μN/nm, and hardness by 0.27 GPa in bones. The reverse problem-solving method also effectively approximates yield stress, yielding results comparable to direct calculations that eliminate the requirement for another destructive testing. The findings also highlight the significance of multi-parametric analysis in fracture-risk

	assessment strategies, other than focusing only on bone mineral density for individuals with T2DM.
31.	Experimental evidence of double explosive synchronization in multilayer oscillator networks **T Khatun,** MS Anwar, P Parmananda - Physical Review E, 2026 **Abstract**: Explosive synchronization (ES) is characterized by irreversible transitions to collective coherence in coupled oscillator networks. A recent study [Phys. Rev. Res. 4, 033009 (2022)] has predicted a richer phenomenon, double explosive synchronization (DES), in which a multilayer system exhibits two consecutive discontinuous transitions. Experimental evidence of DES, however, has remained lacking. Here we report the experimental observation of DES using multilayer networks of Wien-bridge oscillators. By coupling a strongly synchronized low-frequency driving layer to a weakly synchronized high-frequency controlled layer and gradually varying the interlayer coupling, we observe two distinct hysteretic transitions accompanied by bistability. Complementary LTspice circuit simulations reproduce the experimental behavior. These results establish DES as a robust and physically realizable phenomenon in multilayer oscillator networks.
32.	Experimental, statistical, and numerical investigation and comparison of bending angle and longitudinal distortion in AA6061 and magnesium M1A alloy sheets using Box-Behnken design in multi-scan laser bending process A Asgharpour…**R Kant,** M Bakhshi-Jooybari, Hamid Gorji - The International Journal of Advanced Manufacturing Technology, 2026 **Abstract:** Longitudinal distortion (CDLD) is an undesirable deformation that occurs in the laser bending process, causing the sheet to deform along the radiation path in the direction of the axis perpendicular to the radiation plane. This deformation can reduce the accuracy of the final part and limit the applications of the laser bending process. The existence of different variables in the laser bending process affects the CDLD and the bending angle. This study was conducted to investigate the effect of five process parameters, including scan speed, laser power, sheet thickness, beam diameter, and number of passes, on CDLD and bending angle, and also to compare these two outputs on AA6061 and magnesium M1A alloy sheets, statistically, experimentally, and numerically. For this purpose, a Box-Behnken Design (BBD) method with 46 experiments was executed using a numerical simulation verified by experimental tests on both AA6061 and magnesium M1A alloy sheets. The results of the numerical models developed based on the Response Surface Methodology (RSM) indicate that the CDLD of the AA6061 sheet is 99.94% less than that of the magnesium alloy sheet. In contrast, the magnesium M1A alloy sheet exhibits a 124% greater bending angle compared to the AA6061 sheet. Analysis of the thermal results revealed that the lower thermal conductivity and specific heat of magnesium M1A alloy sheets resulted in a 36% greater temperature gradient across the thickness. A higher temperature gradient and coefficient of thermal expansion result in greater compressive plastic strain in the heated zone and, consequently, a larger bending angle. The results of the Analysis of Variance (ANOVA) illustrated that sheet thickness significantly impacts CDLD and the bending angle for both AA6061 and magnesium M1A alloy sheets. The findings of this study provide valuable experimental and numerical guidance for conducting the laser bending process to manufacture parts with maximum bending angles and minimum CDLD.
33.	Exploration on highly dynamic graphs **A Saxena, K Mondal** - Distributed Computing, 2026 **Abstract:** We study the exploration problem by mobile agents in two prominent models of dynamic graphs: 1-Interval Connectivity and T -Connectivity Time. The 1-Interval Connectivity model was introduced by Kuhn et al. [STOC 2010], and the T -Connectivity Time model was

	proposed by Michail et al. [JPDC 2014]. Recently, Saxena et al. [TCS 2025] investigated the exploration problem under both models. In this work, we first strengthen the existing impossibility results for 1-Interval Connected dynamic graphs. We then show that, in T -Connectivity Time dynamic graphs, exploration is impossible with (n−1)(n−2) 2 mobile agents, even when the agents have full knowledge of all system parameters, global communication, full visibility, and infinite memory. This significantly improves the previously known bound of n. Moreover, we prove that to solve exploration with (n−1)(n−2) 2 +1 agents, 1-hop visibility is necessary. Finally, we present an exploration algorithm that uses (n−1)(n−2) 2 +1 agents, assuming global communication, 1-hop visibility, and O(log n) memory per agent.
34.	False data injection detection in isolated AC microgrids using Ramanujan's sum and singular value decomposition **M Pandit, S De, R Sodhi** - IEEE Transactions on Industry Applications, 2026 **Abstract:** A novel two-stage strategy is developed in this work to precisely detect and localize cyber attacks (CAs), such as controller hijacking and unauthorized data modification of Distributed Energy Resource (DER). The Stage-1 of the proposal transforms the raw sensor measurements into a domain called Ramanujan's Sum Domain (RSD), capturing the distorted hidden periodicities caused by CAs, owing to RSD's excellent energy conservation properties. In Stage-2, a Singular Value Decomposition (SVD) technique is applied over the RSD transformed data. Sudden changes in rank of the transformed matrix along with a significant increase in the Largest Singular Value (LSV) and its associated energy contained by the dominant left singular vector detects and localizes the CAs in the DER controllers or its neighboring communication links. The efficacy and robustness of the proposed framework is tested under various types of CAs on the IEEE-13 bus distribution system, modelled in RSCAD, and is validated with Real Time Digital Simulator (RTDS) platform integrated with dSPACE 1104 R&D automation controller through Hardware-in-the-Loop (HIL) simulation. A comparative performance analysis with the state-of-the art CA detection method also confirms its superiority.
35.	Fivefold symmetry-retained formation of pentagrammic nanorattles through galvanic replacement with co-reduction DA James, S Shrikanth, V Gupta, **SPP Fuaadh**…A Jaiswal - Small, 2026 **Abstract:** We report a fivefold symmetry-retained transformation of pentatwinned Au@Ag nanorods into non-convex pentagrammic prism nanorattles through galvanic replacement coupled with ascorbic acid-mediated co-reduction. The coupled redox process enables facet-selective growth while preserving the underlying pentatwinned symmetry, yielding hollow nanorattles composed of a solid Au core enclosed within a gold-rich alloy shell featuring five ridged arms and concave pentagrammic caps. High-resolution microscopy reveals anisotropic deposition localized between twin boundaries, while controlled kinetic modulation enables precise control over morphology evolution. The resulting nanostructure exhibits red-shifted and broadened plasmonic modes and significantly enhanced SERS activity relative to rod-shaped analogues. The retention of fivefold symmetry preserves the crystallographic equivalence of the pentagrammic architecture, contributing to a uniform plasmonic response and reproducible SERS performance. These findings establish a coupled galvanic replacement/co-reduction strategy for engineering complex symmetry-retained, concave plasmonic nanostructures with tailored optical properties.
36.	G-quadruplex-driven potassium ion (K^+) sensing at the MoS_2–aptamer biointerface for wearable electrochemical diagnostics **AL Vinod, Tanya, P Shukla, R Gond, P Ramprasad,** B Behera, **D Pal, B Rawat** - IEEE Sensors Journal, 2026

	Abstract: Accurate monitoring of potassium ions (K+) is crucial for maintaining physiological homeostasis; however, reported K+ sensors often suffer from limited sensitivity, narrow detection range, and poor environmental compatibility. Here, we report a membrane-free, biocompatible, and wearable electrochemical biosensor based on hydrothermally synthesized two-dimensional MoS2 functionalized with a thiolated thrombin-binding aptamer (TBA) for real-time K+ monitoring. The correlated FTIR and cyclic voltammetry (CV) analysis reveals that K+-induced aptamer folding modulates MoS2 interfacial charge-transfer kinetics, which enables a wide detection range of 0.1-100 mM with high sensitivity of 28.20 µA/mM for 0.1-20 mM and 5.40 µA/mM for 40-100 mM. The proposed sensor exhibits excellent selectivity toward K+ with minimal interference from physiologically relevant competing species, including glucose, Cl−, NH+4 , lactate, urea, Mg2+, Na+, Ca2+, and albumin for enabling reliable detection under biologically relevant conditions. The sensor also demonstrates strong device-to-device reproducibility and stable thermal performance over a temperature range of 25°C-40°C, along with excellent mechanical resilience and reliable performance in artificial sweat, which collectively validate its suitability for wearable electrolyte-monitoring applications. By uniting 2-D nanomaterial transduction with biologically driven conformational switching, the MoS2-TBA platform establishes a clear pathway toward practical, biocompatible, and clinically relevant wearable K+ diagnostic technologies.
37.	Growth and properties of sputter-deposited Ti-V-Al-C Bi-metallic MAX phase thin films AS Kharb, **A Pandey,** A Dhanda, **N Sardana,** P Singh, AK Mishra, AK Chawla - Ceramics International, 2026 **Abstract:** MAX phases, layered ternary carbides and nitrides combine metallic and ceramic characteristics, offer high thermal stability, electrical conductivity, and damage tolerance, making them attractive for multifunctional coating applications. In this study, (Ti,V) 2 AlC MAX-phase thin films were synthesized on silicon (001) substrate using magnetron sputtering from a stoichiometric TiVAlC target. To the best of our knowledge, this represents the first thin film realization of the (Ti,V) 2 AlC system by physical vapor deposition. Depositions conducted at 600 °C enabled phase formation at far lower temperatures than those required in bulk synthesis. Structural and chemical analyses (GIXRD, Raman, SEM, and XPS) confirmed phase-pure (Ti,V) 2 AlC with its characteristic M 2 AX architecture and near-equimolar Ti:V M-site occupancy. The films exhibited polycrystalline growth with preferential non-(000l) orientation and nanopyramidal surface morphologies consistent with a Volmer-Weber island growth mechanism. Importantly, coatings displayed multifunctional tunability, including band-gap widening with temperature, stable ohmic transport with adjustable resistivity, and a temperature-dependent wetting transition. These findings demonstrate magnetron sputtering as a viable low-temperature route for stabilizing quaternary MAX phases, positioning Ti-V-Al-C system for protective, optoelectronic, and high-temperature device applications. 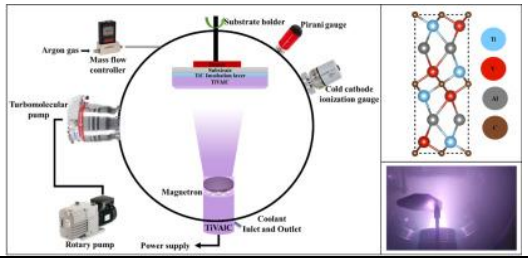
38.	Impact of empagliflozin crystal habits on physicochemical and mechanical properties MD Khan, MH Khan, **A Kumar, N Kumar,** J Haneef - Journal of Molecular Liquids, 2026 **Abstract:** Crystal habit modification plays a significant role in tuning biopharmaceutical as well as mechanical attributes of drug molecules. Different solvent systems (ethanol-water, acetonitrile

	& 1-Butyl-3-methylimidazolium tetrafluoroborate) during recrystallization of empagliflozin (EPG) resulted in three crystal habits, viz. EPG-N (needle shape), EPG-R (rod shape), and EPG-P (plate shape). The influence of the solvent systems on the crystal habit modification was studied using a two-layer interfacial model. Predicted crystal habit in the presence of the solvent systems using this model was well correlated with the experimental outcomes. Modified crystal habits showed different facet growth rate (010) & (001) due to the interaction of the selected solvent systems influencing the crystal habits modification (EPG-N, EPG-R & EPG-P). Solid-state characterization confirms that no polymorphic transformation exists among modified crystal habits. Among them, EPG-R demonstrates the improved apparent aqueous solubility and IDR, as compared to EPG-P and EPG-N, which were correlated with the exposure of hydrophilic functionality on their crystal slices. Additionally, nanoindentation experiments revealed that EPG-P offered better tabletting performance while EPG-R showed greater resistance to permanent deformation, indicating a relatively more brittle mechanical behaviour. These findings give significant insights into the influence of solvent systems on the crystal habit modifications and their overall impact on the physicochemical as well as mechanical properties of the drug molecule.
39.	Impact of infinitely fast reaction on the dynamics of Marangoni flows JS Hong, **L Palodhi, M Mishra,** MC Kim - Physics of Fluids, 2026 **Abstract:** Marangoni flows driven by chemical reactions arise when interfacial tension is modified by reactants or products at an air–liquid interface. We investigate the flow generated by an infinitely fast A þ B! C reaction front using direct numerical simulations, with particular emphasis on the origin and structure of the temporal oscillations frequently observed in such systems. Two nondimensional groups are introduced: a physical Marangoni number, MPhys, capturing hydrodynamic interfacial forcing, and a chemical Marangoni number, MChem, representing surface-tension sensitivity to reaction progress. These parameters enable a unified parametric map from which distinct flow regimes are identified. The results show that the lateral displacement of the reaction front depends primarily on MPhys, whereas temporal oscillations are governed by MChem, which exhibits a well-defined critical value marking their onset. While the reactant concentration ratio strongly influences the dynamics, the reactor aspect ratio affects the flow only during the initial transient. The physical Marangoni effect plays a non-monotonic role, enhancing oscillations at low MPhys but suppressing them at high values. Finally, asymmetric reactivity (b 6¼ 1) substantially lowers the oscillation threshold, whereas symmetric systems remain the most stable. These findings clarify the coupled hydrodynamic–chemical mechanisms underlying chemically driven Marangoni flows and provide a predictive framework for their control.
40.	Improved anticancer efficacy of cisplatin co-delivered with nisin-decorated solid lipid nanoparticles J Kaur, **M Kamboj,** C Misra, K Raza, **B Das**… - Cancer Nanotechnology, 2026 **Abstract:** The therapeutic efficacy of cisplatin is limited by systemic toxicity, acquired resistance, and poor cancer cell specificity. To address these limitations, we developed solid lipid nanocarriers for the co-delivery of nisin and cisplatin (Nis + Cis-SLNs). The developed SLNs exhibited monodisperse spherical morphology, high encapsulation efficiency and sustained release. The therapeutic potential of Nis + Cis-SLNs was evaluated against epithelial malignancies using human epidermoid carcinoma (A431) and breast adenocarcinoma (MCF-7) cells. The nanocarriers demonstrated enhanced cytotoxicity compared to free nisin and cisplatin by synergistically targeting proliferation, apoptosis, and reactive oxygen species generation. Nis + Cis-SLNs triggered an intrinsic apoptotic response by upregulation of caspase-3, Bax, and suppression of Bcl-2. Beyond direct cytotoxicity, conditioned media derived from Nis + Cis-SLNs treated tumor cells were associated with reduced M2 macrophage polarization, suggesting a possible role in immunomodulation of the tumor microenvironment. Collectively, these findings highlight the

	potential of Nis + Cis-SLNs as a promising co-delivery strategy to enhance cisplatin efficacy at reduced doses, potentially improving therapeutic outcomes. 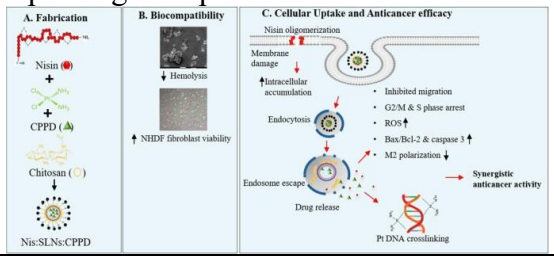
41.	Integrating climate change, land-use dynamics, and explainable AI for future landslide susceptibility assessment in the Western Ghats **S Kushwaha,** B Pradhan, **N James, SR Chavan** - Physics and Chemistry of the Earth, Parts A/B/C, 2026 **Abstract:** With increasing rainfall variability, rapid urbanisation in hilly terrains, and more frequent landslides, there is an urgent need for forward-looking landslide susceptibility mapping (LSM). However, most existing studies focus on historical or current events, with limited assessment of future susceptibility under evolving climatic and land-use conditions. This study projects landslide susceptibility across the Western Ghats, India, for 2021–2100 under four Shared Socioeconomic Pathways (SSPs). Multiple machine learning models were evaluated, and the best-performing XGBoost model, combined with SHapley Additive Explanations (SHAP), was employed for interpretability. The study uniquely integrates future climate projections (CMIP6), projected land-use dynamics, and explainable artificial intelligence (XAI) to produce transparent and scenario-based LSM outputs. Results reveal an overall rise in susceptibility across all SSPs, with the most pronounced increase under SSP5-8.5 during 2051–2100, where 6.38% of the area falls within the very high susceptibility category. Three hotspot zones exhibit marked upward shifts in susceptibility linked to maximum extreme rainfall events. The Kerala region of the Western Ghats shows the most severe deterioration under SSP5-8.5, with nearly two-thirds of hilly areas becoming highly susceptible by 2100. The central and southern zones also show greater susceptibility increases compared to the northern region. By integrating climate projections, land-use dynamics, and XAI, this study provides a novel, transparent framework for future landslide risk assessment and region-specific adaptation planning, offering critical insights to enhance disaster preparedness under changing environmental and socio-economic scenarios. 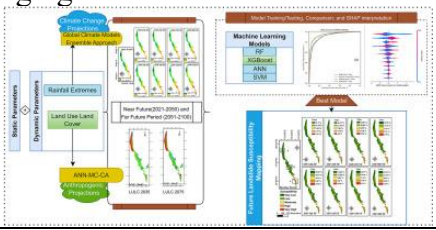
42.	Integrated vertical power delivery–review & challenges M Swaminathan…**R Sharma,** S Kumar - IEEE Transactions on Components, Packaging and Manufacturing Technology, 2026 **Abstract:** This paper reviews and discusses technology advancements required for supporting integrated vertical power delivery in the package. By integrating switching devices, passives (inductors and capacitors) and embedded cooling solutions, this paper argues that high power delivery efficiencies are possible provided the appropriate power delivery architectures are used. The need for early-stage design space exploration along with a co-design framework are also discussed as being essential elements in the quest for achieving integrated vertical power delivery solutions.

43.	Interactive effects of coloured mulches on soil thermal regime, plant growth and yield of tomato under protected and open condition M Farooq…**PP Singh,** S Bansal - Journal of Soil and Water Conservation, India, 2026 **Abstract:** This study was conducted to evaluate the impact of different coloured mulches on soil temperature and yield parameters of tomato crop in open and polyhouse conditions. In this study four different mulch treatments were used as: T1 (Black + Black), T2 (Silver + Black), T3 (Black+Silver) and T4 (without mulch). The highest soil temperature was found in treatment T1 and the lowest temperature value was found in T4 in both polyhouse and open field condition. In treatment T1 the average soil temperature was found 3.9° higher than T4 under polyhouse condition and 3.4° higher in T1 treatment than T4 under open field conditions, respectively. The overall average temperature in T1, T2, T3 and T4 was found to be 22.70, 20.80, 21.78 and 18.70, respectively in polyhouse conditions and 21.50, 19.56, 20.49 and 18.04 under open field conditions, respectively. The fruit yield per plot was found to be higher in treatment T2 as 168kg, followed by treatment T3 as 137kg, T1 as 122kg and lowest value in T4 as 79kg under polyhouse conditions. Similar trend was observed under open field with highest value in treatment T2 as 111kg, followed by T3 as 101kg, T1 as 95kg and lowest value in T4 as 54kg. Thus, mulching helps in regulating the soil temperatures which leads to better yield and early production of crop. The result revealed that silver mulch results in significantly better yield in comparison to black mulch, it improves light reflection and enhances photosynthesis of crop.
44.	Interfacial amine engineering unlocks enhanced MRI relaxivity in silica-coated hematite nanoparticles P Kadian…**Y Bhardwaj,** S Srivastava…**MK Pandey,** JK Randhawa - Analytical Chemistry, 2026 **Abstract:** Engineering the surface architecture of MRI contrast agents is fundamental to achieving superior contrast efficiency and multifunctional therapeutic capability. We report the silica-coated hematite (SIO) functionalized with amine groups via (3-aminopropyl) trimethoxysilane (APTMS) to assess their effects on MRI relaxivity and redox activity. Upon amination, the transverse relaxivity (r_2) increased from 6.20 ± 0.02 to 44.8 ± 0.1 mM^{-1} s^{-1} at 1.5 T. Notably, the prepared hematite nanoparticles exhibit exceptionally high relaxivity, among the highest reported for hematite systems. The higher transverse relaxivity shows that they could be excellent T_2 MRI contrast agents. In contrast, SIO exhibited enhanced hydroxyl radical generation and greater glutathione (GSH) depletion, indicating superior Fenton-like catalytic activity compared to amine-functionalized silica-coated hematite (SIOA). These results show an important design trade-off: surface coatings make MRI relaxivity and biocompatibility better, but they also make poor ROS-mediated therapeutic potential. This study elucidates the mechanisms by which surface chemistry influences dual imaging and treatment efficacy, offering foundational concepts for the development of multifunctional MRI contrast agents in cancer theranostic. 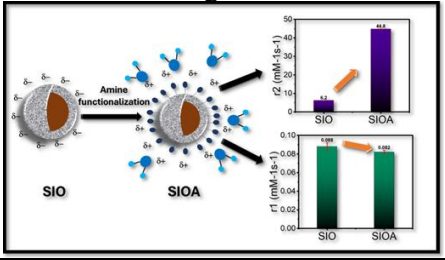
45.	Investigating fission fragments in the 12C+193Ir→205Bi* reaction at *E*lab≈6.2–6.9MeV/nucleon **R Kaur, Amanjot, Priyanka, M Kaushik,** MK Sharma, **PP Singh** - Physical Review **C**, 2026 **Abstract:** The production cross sections of 23 fission fragments in the mass range 71≤ *A*≤141 have been measured in the 12C+193Ir reaction

	at Elab=83.99±0.013, 80.99±0.007, and 74.82±0.026MeV using the recoil-catcher activation technique followed by offline γ-ray spectroscopy. The mass and charge distributions of the fission fragments have been analyzed to study the isotopic and isobaric yield distributions. The mass dispersion parameter ($\sigma 2A$) for iodine isotopes is found to be 4.66±0.82, 4.04±0.52, and 3.13±0.39 at Elab=83.99±0.013, 80.99±0.007, and 74.82±0.026MeV, respectively. The charge dispersion parameter (σZ) for iodine isotopes is estimated to be 0.862, 0.799, and 0.709 at the respective energies. It has been observed that the fission fragment mass distribution displays well-described Gaussian functions, consistent with compound-nucleus fission. The variance of the fission-fragment mass distribution has been analyzed as a function of compound-nucleus temperature and found to increase exponentially with it. The variance is strongly influenced by entrance-channel mass asymmetry, highlighting the role of entrance-channel parameters. The present study also explores a linear dependence of mass variance on the deformation parameter ($\beta 2$) of the target nuclei at the same excitation energy for 12C+193Ir and 12C+169Tm systems.
46.	Label-free analysis of osteoarthritic subchondral bone using Raman spectroscopy combined with machine learning **G Uppal, S Khan,** T Goyal, A Kumar, **R Kumar** - Procedia Computer Science, 2026 **Abstract:** Raman spectroscopy (RS) has emerged as a vital tool in biomedical research due to its non-destructive and label-free nature. This laser-based spectroscopic technique enables the simultaneous detection of multiple molecular components, allowing for the chemical characterization of biological samples with minimal or no sample preparation under physiological conditions. However, a key challenge in analyzing Raman spectra of biological samples is the spectral overlap caused by the vibrational modes of different molecules occurring at the same spectral regions. To address this, machine learning (ML) methods—encompassing a range of multivariate and statistical techniques categorized into supervised and unsupervised approaches—are increasingly recognized for their potential. Among them, the Multivariate Curve Resolution-Alternating Least Squares (MCR-ALS) algorithm, a multivariate ML model, has shown promise in deconvoluting the overlapping Raman signals from biological samples. It can extract meaningful spectral profiles corresponding to specific biochemical components and estimate their relative concentrations. In this study, Raman spectral data were collected from osteoarthritic human subchondral bone. Using the MCR-ALS technique, spectral signatures of three major extracellular matrix components—mineral, lipid, and collagen—were successfully separated. Furthermore, the results demonstrated the relative changes in mineral, lipid, and collagen content across the three ICRS grades of osteoarthritic subchondral bone. These findings highlight the potential of the combined Raman–MCR approach to resolve spectral overlap and enhance the elucidation of complex Raman spectra originating from biological samples, offering new opportunities for improved spectral analysis and its application in biomedical research.
47.	Mapping interpersonal hate: A network and mediation analysis of anger, rumination, and grudge **R Gangopadhyay, P Singh** - The Journal of Psychology, 2026 **Abstract:** Hate, an intense negative emotion, can disrupt and damage interpersonal relationships following transgressions. Despite its destructive potential, the psychological mechanism that fuels hate remains poorly understood. Anger has been identified as a primary component of hate, yet anger and hate differ in their appraisal tendencies and motivational goals. This raises a critical question: how does anger contribute to the emergence of hate? To address this, the present study examined the interplay among anger, anger rumination, grudge, and hate. A total of 740 participants completed self-report measures of these constructs. Using network analysis with regularization methods, followed by serial mediation analysis, we mapped the structural relations among the variables and tested directional pathways. Network analysis revealed grudge as the most central and influential variable showing the highest strength, betweenness, and closeness indices.

	Further, serial mediation analysis revealed that the relationship between anger and hate is serially mediated by anger rumination and grudge. These findings suggest that when anger is not regulated effectively, it may intensify through ruminative thinking and unresolved grudges, resulting in hate. The findings highlight the importance of targeting the maladaptive anger process, particularly rumination and unresolved grudges, in interventions designed to prevent interpersonal anger from transforming into hate.
48.	MBCE: Multi-band contrastive encoding for frequency-aware ultrasound representation learning S Dubey, **T Meena,** D Mahapatra, B Bozorgtabar, S Roy - IEEE Access, 2026 **Abstract:** Ultrasound imaging relies on high-frequency sound waves to visualize internal anatomy in a non-invasive manner, yet automated analysis remains difficult due to low signal-to-noise ratios, speckle artifacts, and inconsistencies across scanners. These challenges are compounded by the scarcity of annotated datasets, limiting feature extraction and generalization across anatomical regions. Conventional self-supervised learning (SSL) models, mostly developed for natural images, often overlook spectral characteristics that are important in ultrasound and may therefore learn representations that are sensitive to scanner- and acquisition-dependent variations. To address this gap, we propose Multi-Band Contrastive Encoding (MBCE), a spectral contrastive learning framework designed to learn frequency-aware ultra-sound representations. MBCE extracts spatial features while incorporating log-magnitude Fourier sub-band features through a shared ResNet-50 backbone enhanced with lightweight cross-attention, enabling joint modeling of spatial and spectral information without separate encoders for each view. We further introduce Spectral-Band Contrastive Loss (SBCL), which aligns low-, mid-, and high-frequency embeddings from the same image while contrasting them against embeddings from other images. Experiments on breast, liver, and pancreas ultrasound datasets show consistent improvements over representative SSL baselines, including cross-organ evaluation on an unseen liver dataset. By explicitly leveraging spectral structure, our approach offers a label-efficient direction for ultrasound representation learning and motivates future evaluation on tasks such as segmentation and detection with larger data corpora. 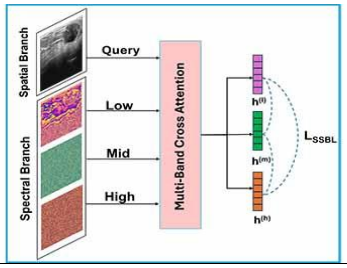
49.	Molecular engineering of minimalistic amphiphilic peptidomimetics for the design of biocompatible hydrogels with potential antibacterial activity S Singh, **P Bundel**…**Y Singh,** R Misra - Biomacromolecules, 2026 **Abstract:** Peptidomimetics have long been of interest in drug discovery; however, their use in the design of higher-order supramolecular structures is limited. Herein, we report the higher-order supramolecular self-assembly of rationally designed ultrashort cationic peptidomimetics by harnessing the unique conformational preferences and enhanced molecular interactions of homologated noncanonical γ- and β-hydroxy-γ-amino acid residues. The intrinsic amphiphilic character of these peptidomimetics drives their self-assembly into fibrillar, viscoelastic, injectable hydrogels with distinctive conformational and supramolecular organization. Furthermore, systematic structural engineering of peptidomimetics yielded a hydrogel matrix with a more hydrated microenvironment conducive for the culture of L929 fibroblast cells. Moreover, the cationic fibrillar networks exhibited potent antibacterial activity, highlighting their potential as

	biocompatible antimicrobial biomaterials. This study demonstrates the importance of rational structural engineering of ultrashort peptidomimetics for the generation of functional biomaterials. 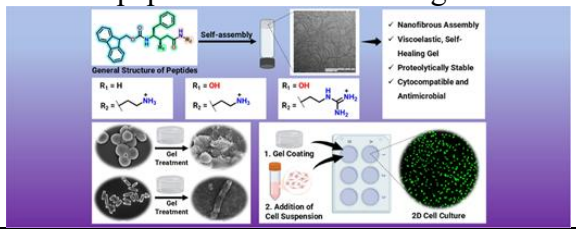
50.	Multifunctional membrane for dyes removal and pathogen inactivation in textile effluent **R Devi, S Jaswal,** R Dhir, J Singh, A Singh, N Kaur, **N Singh** - ChemCatChem, 2026 **Abstract:** Water pollution has become a global health threat. According to WHO estimates, unsafe water is responsible for approximately 1.4–3.5 million deaths annually. Microbial pollutants and resistant organic dyes are frequently not successfully removed by conventional wastewater treatment methods. In addition, coliform bacterial pollution can turn water into a vector for disease transmission, increase organic and nutrient loads, and accelerate antimicrobial resistance. Therefore, to overcome these problems, we present the synthesis of a new copper-metal-ion-based co-crystal (CuCoXtal), which exhibits the ability to reduce dyes and 99% antibacterial efficacy against *Staphylococcus aureus* and *Escherichia coli*. When exposed to UV light, this cocrystal shows exceptional photocatalytic activity, efficiently degrading a range of dyes from textile effluents, including methylene blue, methyl orange, trypan blue, and congo red. At pH 8.5, degradation efficiency increases significantly, indicating that alkaline media generate more reactive oxygen species (ROS), than neutral (pH 7) or acidic (pH 5.5) conditions. Furthermore, a CuCoAXtal@PAM polyamide membrane was successfully fabricated and degraded methylene blue under UV light within 30 min. In addition to its photocatalytic activity, the fabricated membrane serves as an advanced wastewater treatment material that degrades dyes, disinfects, and detoxifies wastewater in a single step. 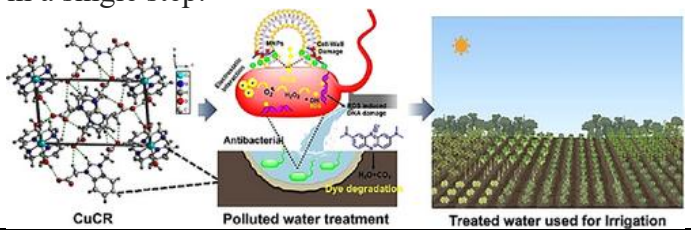
51.	Multiscale spectral-temporal fusion network for crop mapping using sentinel-2 time series image **WT Olani, N Goel** - IEEE Geoscience and Remote Sensing Letters, 2026 **Abstract:** Satellite image time series (SITS) from Sentinel-2 provide valuable temporal information for crop-type mapping. However, most existing approaches model crop phenology at a single temporal scale and may miss complementary short-term, seasonal, and annual dynamics. To address this limitation, this letter proposes a Multiscale Spectral–Temporal Fusion Network (MSTFN) for pixel-wise crop classification from Sentinel-2 time series. MSTFN uses Conv1D for local variations, BiLSTM for seasonal dynamics, and Transformer-BiLSTM for annual dependencies. An inter-scale self-attention module adaptively fuses these representations to support crop discrimination under overlapping temporal-spectral signatures. On the TimeSen2Crop benchmark, MSTFN achieves 87.85% OA and 86.81% WF1, showing competitive-to-improved performance over representative CNN, recurrent, and attention-based baselines.
52.	Multivariate measures of critical transitions in a bistable gene regulatory network **SN Chattopadhyay, AK Gupta** - Chaos: An Interdisciplinary Journal of Nonlinear Science, 2026

	Abstract: Developing concise gene regulatory networks that accurately encode cellular decision-making processes remains a key area of research across biological dynamics. Here, this challenge is addressed by investigating the behavior of a minimal gene regulatory network comprising three transcription factors within deterministic and stochastic frameworks. The components of the network interact through self-activation of a single transcription factor, mutual inhibition between a pair, and additional cross-inhibition exerted by the third. Following a brief mathematical analysis of the deterministic model, the influence of parameter variations on the steady-state concentrations of the transcription factors is quantified using Sobol's sensitivity method. The subsequent bifurcation analysis, conducted by varying the most sensitive parameter, reveals three distinct bistable configurations: isola, mushroom, and canonical toggle. Thereafter, basin stability quantifies the resilience of coexisting attractors, demonstrating that inhibitory strength can shift stability in favor of one state. In addition, 12 multivariate statistical indicators are computed using different strategies to anticipate emergent critical transitions within the mushroom architecture. Their predictive efficacy is systematically evaluated across four different criteria. First, sensitivity analysis reveals that the predictive performance of principal component-based indicators, along with the mutual interdependence-based measure, remains less affected by variations in the hyperparameter configurations. Statistical significance testing further demonstrates the superior efficacy of multivariate indicators in capturing the transition from the upper to the lower branch of the mushroom, compared with the reverse case. These results are further justified by a detailed robustness assessment and false-positive detection test. Taken together, this work bridges contemporary gene regulatory dynamics with the prediction of critical transitions, introducing methodologies that have not been previously applied in this context.
53.	Nonlinear charge density fluctuation-driven plasmonic enhancement in Au–Ag thin films **J Singh, P Rani, R Dahiya**, **M Kumar,** NK Gupta, **S Sarkar** - ACS Applied Electronic Materials, 2026 **Abstract:** Bimetallic alloys of gold and silver have gained considerable attention due to their broad utility in catalysis, biomedicine, and optical technologies, owing to their enhanced surface plasmon polariton (SPP) quality factor compared to the corresponding pure metals. Earlier attempts to understand the central reason for this improved performance, despite their noncommensurate stoichiometries, have not yielded a clear picture. To address this, we performed spectroscopic ellipsometry together with Hall measurements on composition-controlled, equal-thickness Au–Ag alloy films. By examining the interdependence of plasma frequency, carrier concentration, and effective mass, we found that a nonlinear rise in carrier density is the dominant factor behind the improved optical response. To further understand this anomalous carrier density behavior, the Mayadas–Shatzkes (MS) model was applied, revealing how polycrystallinity and grain-boundary scattering influence charge-transport dynamics in the alloys. Additionally, the composition-dependent nonlinear trends in the extracted physical parameters were modeled using a bowing-type polynomial mixing approach. This combined experimental–theoretical framework not only aligns the measured results with a consistent physical model but also accounts for discrepancies based on the MS formalism. By establishing a direct link between microstructural effects, electronic properties, and optical response, this study resolves the origin of the nonlinear optical behavior observed in stoichiometric ratios of bimetallic thin films. 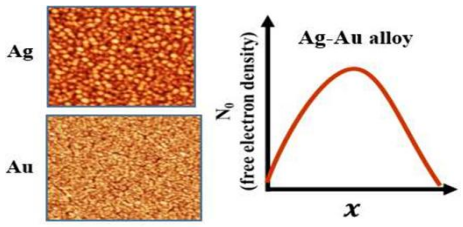

54.	On-chain heuristic dynamic swarm-based bi-directional stacked MLP framework for smart industrial pollution mitigation S Dey, **S Mishra,** AS Prasad, D Ramesh - IEEE Transactions on Engineering Management, 2026 **Abstract:** Air quality is deteriorated by industrial operations, which present a serious threat to environmental health and sustainable development. Predictive models that can efficiently assess and mitigate industrial pollution in real-time are therefore desperately needed as multivariate time-series data become more readily available. Therefore, we offer the On-Chain Heuristic Dynamic Swarm-based Bi-directional Stacked MLP Framework for Intelligent Industrial Pollution Reduction (OraacLe) to meet this need. OraacLe combines bi-directional stacked multilayer perceptron (Bi-SMLP) neural networks with heuristic dynamic swarm optimisation. OraacLe offers transparent, adaptive learning for industrial air pollution mitigation in an hourly, on-chain environment. In contrast to existing methods that generate static predictions and offer limited optimisation, such as Multilayer Perceptron (MLP), Support Vector Regressor with Quasi-Linear Kernel (SVR with QLK), Nested Long Short-Term Memory (NLSTM), Recurrent Air Quality Predictor (RAQP), CNN LSTM, Temporal Convolutional Networks (TCN) and Trans former OraacLe allows continuous forecasting, analysis, and mitigation of industrial air pollution levels, supporting proactive decision-making. Experiments show that OraacLe boosts fore casting accuracy by 44.5%, improving performance from 0.647 (Transformer) to 0.935 at the 12-hour horizon. It maintains 68.2% robustness under 20% Gaussian noise, outperforming TCN (52.3%), while reducing MAE from 1107.92 to 0.60 and in creasing R2 custom from 0.641 to 0.807, demonstrating effectiveness for long-horizon forecasting and noise resilience in air pollution mitigation. Also, the methodological rigour of the proposed approach is demonstrated through extensive robustness checks, including noise-perturbation analysis, ablation studies, and multi metric evaluation across both synthetic and real-world datasets. based on how plants actually behave. It helps regulators conduct objective, accurate compliance inspections, speeds up the issuance of alerts, and makes it easier to create emission levels that adapt to operational conditions. Consequently, OraacLe connects sophisticated forecasting technology with practical operational requirements. It provides policymakers with reliable information to create adaptable, sustainable regulatory frameworks and empowers engineering managers to take prompt action when emissions deviate from targets.
55.	On the behaviour of cycle integrals of j invariant **B Kumar, J Kumari** - Mathematika, 2026 **Abstract:** In this paper, we study the values of modular functions at real quadratic irrationalities which are defined in terms of cycle integrals of modular functions associated with closed geodesics. We refine a result of Bengoechea and Imamoğlu to include values (and its limiting behaviour) of modular functions at a larger class of real quadratic irrationalities. As a consequence, we deduce the limiting behaviour of values of modular functions at powers of Pisot–Vijayaraghavan numbers. Further, we deduce distribution of class numbers of real quadratic fields having discriminants of a particular type.
56.	On traces of cycle integrals attached to harmonic weak Maass forms V Kalia, **B Kumar** - Journal of Number Theory, 2026 **Abstract:** Bringmann, Guerzhoy and Kane introduced the notion of traces of cycle integrals of harmonic weak Maass form of negative weight in terms of traces of weak Maass form of weight 0. They proved that these traces coincide with the traces of cycle integrals of the associated classical cusp forms. Their result applies to the case of positive discriminants d , δ such that dδ not a square. In this paper, we define traces of cycle integral of weak Maass forms of weight 0 in the case of negative discriminants d, δ such that dδ not a square and prove the similar result. Further,

	we define modified traces of weak Maass forms of weight 0 in the case of discriminants d , δ such that dδ a square and prove that for a given harmonic weak Maass form of negative weight, the modified traces of cycle integral of the associated weak Maass form of weight 0 coincides with the twisted central L -values of the associated classical cusp forms. As an application of our result, we classify all weakly holomorphic modular forms lying in the space of harmonic weak cusp forms in terms of vanishing of modified traces (twisted central L -value).
57.	Optimization of β2 and β4 deformations for 176Yb using quasi-elastic barrier distribution G Ram, MK Sharma…**Amanjot**…**PP Singh,** BP Singh - Nuclear Physics A, 2026 **Abstract:** An effort has been made to optimize the quadrupole and hexadecapole deformation parameters for 176 Yb nuclei from the barrier distribution derived from quasi-elastic scattering measurements.The quasi-elastic excitation functions for the 14 N+ 176 Yb system were measured using the HYbrid Telescope ARray (HYTAR) detecting setup in the General Purpose Scattering Chamber (GPSC) at the Inter-University Accelerator Centre (IUAC), New Delhi. The barrier distribution for 14 N+ 176 Yb has been derived from the measured excitation functions. The experimental observables have been interpreted in light of full coupled channel calculations using the quantum mechanical code FRESCO. The coupled channel calculations for 14 N+ 176 Yb suggested that 176 Yb behaves as a rotational nucleus, and coupling up to the first three excited states with reported values of β 2 and β 4 explains the observed shape of the barrier distribution well. However, the deviation of coupled channel calculations from the precisely measured barrier distribution is further anticipated to have uncertain values for the considered deformation parameters, which have not been precisely reported in previous studies. The values of the deformation parameters β 2 and β 4 have been extracted using the chi-square minimization method. It has been found that β 2 =0.306 and β 4 = − 0.043 yielded the best fitted values to the experimental data. The present work strongly infers negative values for the hexadecapole deformation of 176 Yb and reports the values of β 2 =0.306 ± 0.002 and β 4 = − 0.043 ± 0.003 confidently up to three decimal places, which are consistent with those reported in the literature. Moreover, the optimized values have been corroborated by the angular distribution and fusion excitation function. The successful reproduction of the experimental observables, the angular distribution and fusion excitation function, through coupled channel calculations, substantiates the optimized values.
58.	Paley-Wiener theorem for Weyl transform of radial function A Samanta, **S Sarkar** - Advances in Mathematics, 2026 **Abstract:** The main purpose of the paper is to prove the following Paley-Wiener type theorem for “spherical Weyl transform” of radial function which is in the same spirit of classical Paley-Wiener theorem for Euclidean Fourier transform. Let f be a square integrable radial function on C d and f ˜ denotes its “spherical Weyl transform” (which is a complex-valued function defined on the set {2 k + d: k = 0, 1, 2, ⋯}). Then f is compactly supported with support inside the (closed) ball of radius R centred at origin iff its spherical Weyl transform f ˜ extends to an entire function on C such that f ˜ (z 2) is exponential type ≤ R . Also, using this theorem we obtained a decent Paley-Wiener theorem for the spherical Fourier transform on the Heisenberg group
59.	Perception of instructors and students on kalarippayattu: A mixed-method study on an Indian martial art **AV Suresh, A Nandha** - Asian Journal of Sport History & Culture, 2026 **Abstract:** This paper aims to study the perception of kalarippayattu, an Indian martial art form, founded on the views expressed by instructors and students in the southern Indian state of Kerala. Speculated to have sustained through antiquity, the origins of this martial art form are shrouded in mythical tales. Despite its rich history, kalarippayattu has not gained its due academic interest from martial arts scholars. It is in this context that this study propounds a mixed-methods approach to

	analyse the contemporary perception of kalarippayattu among practitioners. The participants of the study include kalarippayattu instructors and students practising kalarippayattu. The study analysed participants' perception of changes in pedagogy and elicited supportive and critical observations on various aspects of kalarippayattu like health benefits, motivation of practice, challenges and suggestions for future growth. Correspondingly, the philosophy that dictates kalarippayattu is rooted in dharma, the Indian concept of ethics. Dharma in kalarippayattu extends beyond individual duties and responsibilities towards personal growth. The practitioner is trained to be committed to the larger society. The findings also highlight the positive perception of this martial art among its practitioners signifying the importance of the preservation and revival of kalarippayattu.
60.	Physics-informed adversarial networks for stochastic second-order mean-field games of autonomous traffic **NK Pande, A Kumar, AK Gupta** - Royal Society Open Science, 2026 **Abstract:** Inspired by the highly complex and nonlinear traffic flow phenomenon, we propose a second-order continuum model for autonomous vehicles (AVs) by considering them as rational and utility-optimizing agents. Further, by accounting for stochastic fluctuations in driving dynamics, a non-cooperative differential game problem is converted to a mean-field game (MFG) system comprising a forward-in-time second-order continuity equation (CE) and a backward-in-time parabolic Hamilton–Jacobi–Bellman (HJB) equation. By formulating various driving cost functions, we generate two non-separable stochastic MFG systems. Next, a modified generative adversarial network (GAN)-based machine learning (ML) model is proposed as a surrogate to learn the dynamics of the proposed MFG systems. The proposed GAN comprises three physics-informed neural networks (PINNs) that compete with each other until an approximate equilibrium is attained. We validate our results on both the simulated and real-world datasets.
61.	Plane wave propagation in an elastic solid undergoing uniform angular acceleration D Rani, S Goyal…**SC Martha** - Journal of Vibration Engineering & Technologies, 2026 **Abstract:** Purpose The present study investigates the propagation characteristics of plane waves in an infinite elastic solid undergoing uniform angular acceleration. The objective is to examine how angular acceleration modifies the dispersion behaviour, attenuation properties, and polarization characteristics of elastic waves in a rotating medium. Methods The analysis is carried out within the framework of linear elasticity by incorporating the additional inertial coupling term associated with angular acceleration into the governing equations of motion. A time-harmonic plane-wave solution is assumed under the local-time approximation, and the resulting dispersion relation is obtained from the corresponding determinantal equation. The phase speeds, attenuation coefficients, and particle-motion characteristics are then analysed for a representative elastic material. Results It is shown that three distinct propagating wave modes may exist whose characteristics depend on the angular velocity, angular acceleration, frequency, and direction of propagation. In general, the waves are neither purely longitudinal nor purely transverse; instead, rotational effects introduce coupling between dilatational and shear motions, leading to quasi-dilatational and quasi-shear behaviour. For special propagation directions relative to the axis of rotation, the classical longitudinal and transverse waves are recovered as limiting cases. Conclusion The results demonstrate that uniform angular acceleration significantly influences the dispersion and attenuation characteristics of elastic waves. The formulation consistently reduces to the known solutions for non-rotating and uniformly rotating elastic solids, thereby validating the present analysis.
62.	Polarization-independent dichroic beam splitter using all-dielectric metasurface at near-infrared wavelength C Kumar, BK Bhowmik…D Sikdar, **G Kumar** - Advanced Theory and Simulations, 2026

	Abstract: In the modern era, metasurfaces have gained significant attention for their potential in light manipulation, including focusing, bending, blocking, and wavefront control, as well as designing ultra-thin optical components. Metasurfaces comprising high-index dielectric nanostructures have emerged as an inevitable platform for high-performance flat optical devices. Among these, a dichroic beam splitter is a crucial optical component that selectively reflects and transmits light based on the wavelength, enabling precise control over beam routing. In this work, we demonstrate a polarization- and angle-tolerant metasurface-based dichroic beam splitter that operates as a harmonic separator, efficiently separating the fundamental wavelength (1560 nm) and its second harmonic (780 nm) wavelength. Using a 2D array of gallium phosphide (GaP) cylindrical nanostructures, the proposed device exhibits high transmission at 1560 nm while simultaneously achieving near-unity reflection at 780 nm over a bandwidth of approximately 168 nm. This device finds application in fluorescence microscopy, multispectral imaging and advanced laser systems due to its precise spectral selectivity in the near-infrared regime. Beyond these applications, our result highlights a versatile design route to compact dichroic beam splitters that can replace conventional bulky optical devices, with promising prospects for on-chip photonics and portable optical elements.
63.	Printability of 3D-printed concrete with emphasis on buildability: A scientometric and thematic review S Barbhuiya, BB Das, **AS Rajput**…AK Das - Journal of Materials in Civil Engineering, 2026 **Abstract:** This paper presents a comprehensive scientometric analysis and thematic exploration of research trends in three-dimensional (3D) printed concrete (3DPC), with a particular focus on the interrelated concepts of buildability and printability. Following an overview of the background and significance of 3DPC in modern construction, the study emphasizes the critical roles of buildability and printability in determining the success and structural integrity of printed elements. Utilizing bibliometric data from Scopus, tools such as VOSviewer were employed to analyze publication trends, influential authors, institutions, and keyword patterns. The analysis reveals increasing research activity, with notable global collaboration and thematic evolution over time. Subsequent sections delve into the definitions, influencing factors, testing methodologies, and challenges associated with both buildability and printability. Recent advancements, experimental techniques, and real-world case studies are examined to highlight technological progress. The study further explores the synergies and trade-offs between buildability and printability, proposing integrated frameworks for material and process optimization. Finally, the paper identifies current research gaps and outlines future directions, emphasizing the need for interdisciplinary approaches and standardization. The findings aim to guide researchers and practitioners toward more efficient, reliable, and scalable 3DPC applications in the construction industry.
64.	Random silicon micromirrors for enhanced emission rate and spin readout contrast of NV centers **M Aleem, N Singh, R Dhankhar, RV Nair** - Advanced Optical Materials, 2026 **Abstract:** The nitrogen-vacancy (NV) center in diamond exhibits spin-dependent optical response at room temperature, making it a driving force in quantum computing, memory, and sensing. In practice, shot-noise magnetic sensitivity is often constrained by very low collection efficiency, dephasing, and spin contrast, which calls for broadband emission enhancement. Here, we present broadband engineering of the NV center emission using a random array of silicon (Si) micromirrors, acting as nanocavities. We observe broadband emission enhancements, increased spin-readout contrast, and reduced linewidth, thereby enhancing magnetic sensitivity for an NV-based quantum sensor. The experimental and simulation results demonstrate broadband Purcell enhancement, resulting in a two-fold reduction in the emission lifetime. We even observe a stronger lifetime reduction, exceeding four-fold, accompanied by an intensity enhancement of

	more than ten-fold. An improved signal-to-noise ratio in the spin readout contrast is observed with an eight-fold improvement in magnetic sensitivity for NV centers coupled to Si micromirrors. The results confirm that random Si micromirrors demonstrate a practical, fabrication-tolerant route to achieve broadband emission enhancement and more sensitive quantum sensors**.**
65.	Reg-GelNet: Deep learning receiver for asynchronous distributed chirp spread spectrum **A Gupta, Irtizah, S Agarwal** - IEEE Communications Letters, 2026 **Abstract:** Asynchronous distributed chirp spread spectrum (AD-CSS) enables cooperative long-range, low-power Internet of Things (IoT) communication but suffers from independent time, frequency, and phase offsets, leading to non-coherent signal addition and degraded detection performance. Conventional receivers relying on explicit offset and channel estimation become computationally burdensome and inaccurate in such settings. To address this, we propose Reg-GelNet, a deep learning–based receiver that performs offset and channel compensation along with symbol detection. Reg-GelNet uses a deep neural network (DNN) to mitigate signal impairments, a Gel'fand transform for compact time–frequency feature extraction, and a convolutional neural network (CNN) for symbol classification, removing the need for explicit synchronization or channel estimation. Simulations show that Reg-GelNet achieves markedly lower bit error rate (BER) than state-of-the-art receivers while maintaining low complexity, offering an efficient and practical solution for asynchronous IoT networks.
66.	Roadmap on structured light lasers Q Liu, X Fu, Z Zhang…Q Sheng, W Shi, J Yao, **V Pal**…Y Shen - Journal of Optics, 2026 **Abstract:** How to further increase the information capacity carried by structured light by extending and coupling many degrees of freedoms of light over time and frequency domains, such as polarizations and spatial structures, is one of the frontiers in optics and photonics. Diffraction and transformation optics have already made the generation of structured light full of flexibility, while, considering the efficiency and compactness of the system, the structured light directly generated from lasers is greatly in need as the "at-the-source" solutions. It is a booming direction to customize diversified structured light easily and precisely generated from exquisitely designed lasers. This roadmap intends to highlight the recent advances in the classical strategies and novel designs for structured light lasers, including the cavity parameters direct modulations, new optical elements assisted modulations, on-chip micro/nano-cavity designs, as well as the multiple applications of the structured light laser, presenting a bird's eye viewpoint on the development of structured light lasers and the outlook of future trends and open challenges.
67.	Robust mean field game of autonomous vehicles on multilane roadways via attention-based adversarial networks **NK Pande, A Kumar, AK Gupta** - Proceedings of the Royal Society A: Mathematical Physical and Engineering Sciences, 2026 **Abstract:** Drawing inspiration from the highly complex and nonlinear traffic flow phenomenon, first a model for the movement of autonomous vehicles (AVs) on multilane roadways, based on a robust mean field game (MFG) framework, is formulated. By considering the effect of adversarial disturbances in the traffic dynamics along with the effect of uncontrollable noise in the lateral movement of the vehicles, a min–max optimal control problem is converted to a coupled system of forward-in-time Fokker–Planck–Kolmogorov (FPK) and backwards-in-time Hamilton–Jacobi–Bellman–Isaacs (HJBI) equations. By formulating various cost functions, an equilibrium and a non-equilibrium (ML) model is developed, and their link with traffic flow is described. Second, a generative adversarial network (GAN)-based machine learning model is proposed as a surrogate tool for modelling the dynamics of the robust MFG framework. The GAN model is equipped with two physics-informed attention-based frameworks followed by a residual-based adaptive sampling

	strategy to enhance the learning efficiency and improve the accuracy. The validity of the model is tested against the synthetically generated traffic flow scenarios.
68.	Semantic labeling with fulfillers in multilingual contexts K Pala, V Nedumpozhimana, **S Shalu** - Frontiers in Language Sciences, 2026 **Abstract:** This paper introduces a novel approach to semantic labelling grounded in the fulfiller concept—a cognitive-semantic theory that highlights the role of absent but contextually inferred elements in meaning construction. We argue that prevailing semantic labeling practices often neglect this essential aspect of meaning, especially in typologically diverse languages where semantic roles may be implicit, elided, or heavily reliant on contextual inference. Drawing on a small pilot multilingual corpus, we undertake a qualitative, manually annotated study to identify and classify fulfillers—semantic roles that are not overtly expressed but are grammatically, discursively, or culturally implied. Our analysis focuses on languages with pro-drop characteristics, argument ellipsis, and context-dependent expression, revealing systematic patterns in how meaning is fulfilled through absence. The findings suggest that accounting for fulfillers can deepen our understanding of cross-linguistic variation in argument realization and semantic structure. We discuss implications for typological theory, annotation methodology, and potential future integration into computational models. This work opens a new direction in semantic labeling by foregrounding the cognitive and typological relevance of semantic absences.
69.	Short-range lattice correlation induced anomalous light transmission in photonic structures **M Aleem, RV Nair** - APL Engineering Physics, 2026 **Abstract:** Long-range lattice correlations are essential for forming bandgaps in electrons, phonons, and photons. Consequently, disorder has often been viewed as detrimental to bandgap formation, with the ideal system being a perfect crystal free of lattice imperfections. However, recent studies have shown that short-range lattice correlations in disordered media can produce photonic bandgaps. Here, we investigate tunable short-range lattice-correlation-induced photonic bandgaps in low-index-contrast samples with correlations extending up to 2 μm. Reflectivity measurements reveal resonant peaks and corresponding transmission dips that closely match the calculated structure factor, indicating a frequency gap. Angle- and polarization-dependent reflectivity measurements confirm a broad, scalable bandgap in good agreement with simulations, with a significant reduction in the local density of optical states. The light-transmission measurements across frequencies below, within, and above the bandgap exhibit an unexpected transmission decay due to short-range lattice correlations. The spectral-dependent transport mean free path shows strong suppression within the bandgap and enhancement near the band edges, consistent with theoretical predictions. Our results provide new insights into the role of short-range correlations and their potential for applications in emission control, structural coloration, and passive radiative cooling systems.
70.	Simultaneous TCR and IL-2 agonism selectively enhances epitope-specific CD8 T-cell responses during chronic viral infection M Hashimoto, **MA Khan,** A Akhtar, **JN Agrewala**…R Ahmed - Journal of Virology, 2026 **Abstract:** Interleukin-2 (IL-2) remains an attractive cytokine for enhancing antigen-specific CD8 T-cell responses in cancer immunotherapy, but systemic toxicity hinders its broad clinical application. To address this, various IL-2-based therapeutics have been engineered with altered IL-2 receptor bias or targeted delivery to tumors, the tumor microenvironment, or immune cell populations. Ideally, IL-2 signals should be selectively delivered to antigen-specific CD8 T cells, boosting their responses and promoting effector differentiation while sparing non-targeted populations. Immuno-STAT (Selective Targeting and Alteration of T cells) is a fusion protein platform comprising a bivalent peptide-major histocompatibility complex (MHC) class I complex

	and an affinity-attenuated IL-2 mutein that co-stimulates T-cell receptor and IL-2 signaling in epitope-specific CD8 T cells. Here, we investigated whether a D^bGP_{33-41}-targeted Immuno-STAT enhances D^bGP33-specific CD8 T-cell responses in a mouse model of chronic lymphocytic choriomeningitis virus infection. Immuno-STAT treatment selectively expanded D^bGP33-specific CD8 T cells with an effector-like phenotype. Non-targeted D^bGP276-specific CD8 T cells showed little to no expansion in response to D^bGP_{33-41}-targeted Immuno-STAT therapy, underscoring the selectivity of this approach. However, minor changes in phenotypic markers, including increased expression of CD25 and CX3CR1, were observed in non-targeted CD8 T cells, likely reflecting bystander IL-2 signaling. Combining Immuno-STAT with PD-1 blockade augmented D^bGP33-specific CD8 T-cell responses more effectively than PD-1 blockade alone, with minor effects on the non-targeted D^bGP276-specific population. These findings inform the clinical development of Immuno-STAT and other IL-2 therapeutics and highlight the value of coordinated TCR and IL-2 stimulation during chronic antigen exposure, alone or in combination with PD-1 blockade.
71.	Special issue on advances in analysis, algebra and applied mathematics H Nagar, N Mani, R Shukla, N Alias, **J Kumar** - Journal of Interdisciplinary Mathematics, 2026 **Abstract:** This special issue on "Advances in Analysis, Algebra and Applied Mathematics" brings together contemporary research contributions addressing emerging challenges and opportunities in modern mathematics. It places particular emphasis on areas such as thermoelasticity, optimization, fractional calculus, summability theory, fixed point theory, and special functions, highlighting their theoretical advancements as well as their practical relevance to sustainable development. The volume focuses on innovative methodologies and interdisciplinary approaches, including the integration of fractional integral operators with special functions, the application of summability techniques, and the formulation of novel hybrid iterative schemes in fixed point theory. In addition, it presents significant generalizations of classical fixed point results and explores analytical frameworks relevant to thermoelastic models and optimization problems. Through these diverse contributions, the issue aims to highlight the role of advanced mathematical tools in addressing real-world scientific and engineering challenges.
72.	Stochastic game dynamics in tumor metabolism **S Sarkar, S Deb,** JM Drake, **PS Dutta** - Journal of Physics: Complexity, 2026 **Abstract:** Strategic interactions between tumor cells have been hypothesized to arise through evolutionary processes in which cell actions are conditioned on their fitness payoffs. Temporal change in payoffs impacts cell strategies, leading to the evolution of unwanted traits and genetic variation. Consequently, understanding the stochastic game dynamics of tumor metabolism for fluctuating payoffs is an important problem. Here, we study a game-theoretic model of tumor metabolism with fluctuating payoffs. A key feature of this model is the metabolic exploration rate, a quantity that governs metabolic symbiosis in tumor cells and thereby affects tumor progression to metastasis. We find that intrinsic noise induces a transition from a dominance game to a coordination game for an increase in metabolic exploration rate. This transition coincides with a change in the payoffs for the tumor cells at the threshold for critical transitions of the corresponding stochastic system. As a result, our model suggests that variations in payoffs due to intrinsic fluctuations can lead to unexpected changes in tumor cell persistence, transitioning from dominance to coexistence. Additionally, we investigate some candidate early warning signals that we hypothesize may anticipate critical transitions in the stochastic tumor system, guiding therapy to decouple tumor metabolism and thereby prevent cancer proliferation.
73.	Techno-economic assessment of hydrogen-based direct reduction for India's steel sector: Comparative analysis with natural gas DRI and policy enablers **H Kamal,** L Hviid…**AH Sahir** - Sustainable Energy Technologies and Assessments, 2026

	Abstract: The iron and steel sector contributes nearly 7% of the global energy-related CO 2 emissions. In India, this challenge is amplified due to high production of coal based direct reduced iron (DRI) (~80% share). This research evaluates the techno-economic feasibility of hydrogen-based direct reduction (H 2 –DRI) for India's steel industry and benchmarks its results against natural gas-based DRI (NG–DRI), under realistic market conditions. A 1 million tons per annum (MTPA) H 2 –DRI plant and NG-DRI plant is modeled using ASPEN Plus v14, and economic estimates are developed with sensitivity to renewable electricity tariffs, load factor, and policy levers such as carbon pricing and green steel premiums. By comparing DRI based on natural gas, hydrogen and coal the impact of capital expenditure, operational expenditure and overall economics in terms of levelized cost of iron production is evaluated. Results indicate that demand side dynamics like green steel premium and carbon pricing are important factors towards economic viability of H 2 based DRI. 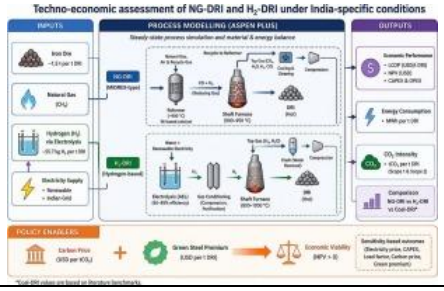
74.	Thermodynamic analysis of membrane distillation under variable solar loading using effectiveness-NTU method for freshwater production **J Dwivedi, KS Chauhan, H Tyagi** - International Communications in Heat and Mass Transfer, 2026 **Abstract:** Water desalination holds considerable promise in addressing the pressing challenges of water scarcity in the contemporary world. This study focuses on performing a comparative thermodynamic analysis of various membrane distillation configurations, including DCMD, AGMD, and VMD, under variable solar loads using the effectiveness-NTU method. The work aims to understand fluid flow behaviour under varying ambient conditions and solar irradiation, along with the influence of geometric and operating parameters. The effectiveness-NTU method has been widely applied to DCMD and AGMD; however, its application to VMD remains limited due to the absence of a conventional cold-side fluid stream and the strong coupling between heat and mass transfer under vacuum conditions. To address this limitation, a novel methodology is developed by introducing a modified overall heat transfer coefficient, wherein the membrane and condenser are treated as a single unit, as both are governed by similar heat transfer mechanisms, namely conduction and latent heat transfer. System performance is evaluated based on distillate mass flux. The findings reveal that system performance is notably enhanced during summer compared to winter. Among the configurations studied, VMD is the most efficient, yielding the highest distillate mass flux. In this study, DCMD and AGMD exhibit mass fluxes that are 20% and 90% lower than VMD, respectively, with AGMD showing the lowest performance. Distillate flux in VMD is significantly influenced by condenser pressure variations. As the pressure increases from 10 kPa to 15 kPa and then to 20 kPa, the distillate flux decreases by 25.9% and 41.1%, respectively. Additionally, during winter, laminar flow on the saline side proves to be superior to turbulent flow across all three configurations. When the saline-side flow at noon transitions from laminar to turbulent, the distillate flux decreases by 66.32%, 32.7%, and 26.5% for DCMD, AGMD, and VMD, respectively. Overall, this study provides new insights into the thermodynamic behaviour of membrane distillation systems under variable solar loading.
75.	Understanding traffic in a hierarchical triangular fractal network

	R Sati, SN Chattopadhyay, AK Gupta - Physica A: Statistical Mechanics and its Applications, 2026 **Abstract:** In recent decades, understanding traffic congestion in highway networks with diverse topological structures has attracted significant attention due to its severe societal and environmental consequences. Motivated by the need to better understand congestion formation in complex transportation systems, this paper introduces a nontrivial hierarchical triangular fractal network containing multiple branching and merging pathways through which vehicles dynamically propagate. Density evolution equations for the initial recursive generations are derived using the widely recognised speed-matching framework, and the resulting traffic dynamics are characterised in terms of the macroscopic variables density and flow. For the zeroth-generation fractal structure, the flow diagrams reproduce the elementary macroscopic fundamental diagram, while the steady-state densities increase linearly with the mean density, as determined analytically and verified numerically. Within the first-generation hierarchical triangular fractal network, increasing vehicular bifurcation progressively reduces traffic asymmetry and drives the self-similar subunits toward the transport behaviour of the parental generation. In the second-generation network structure, increased branching complexity gives rise to heterogeneous density accumulation, skewed flow-density relationships, and node-dependent transport states. The visual observations are further supported by quantitative measures. Phase diagrams further reveal that the distribution of low-density and high-density regimes depends strongly on both the conserved mean vehicle density and the branching coefficients. Overall, the results highlight the crucial role of hierarchical branching in regulating traffic redistribution and congestion formation, and may help identify congestion-prone nodes and develop efficient routing strategies in complex transportation networks.